Global Asymptotic Tracking for Marine Vehicles using Adaptive Hybrid Feedback

Erlend A. Basso♯, *Graduate Student Member, IEEE*, Henrik M. Schmidt-Didlaukies♯, *Graduate Student Member, IEEE*, Kristin Y. Pettersen, *Fellow, IEEE*, and Asgeir J. Sørensen, *Senior Member, IEEE*

***Abstract*— This paper presents an adaptive hybrid feedback control law for global asymptotic tracking of a hybrid reference system for marine vehicles in the presence of parametric modeling errors. The reference system is constructed from a parametrized loop and a speed assignment specifying the motion along the path, which decouples the geometry of the path from the motion along the path. During flows, the hybrid feedback consists of a proportional-derivative action and an adaptive feedforward term, while a hysteretic switching mechanism that is independent of the vehicle velocities determines jumps. The effectiveness of the proposed control law is demonstrated through experiments.**

***Index Terms*— Marine vehicles, hybrid systems, adaptive control, nonlinear systems**

I. Introduction

IT is well known that continuous-time systems whose state-space can be identified with a vector bundle on a compact manifold have no point that can be globally asymptotically stabilized by continuous-time state feedback [1]. This is referred to as a topological obstruction to global asymptotic stability and follows from the fact that no compact manifold is contractible.

Topological obstructions to global asymptotic stability can be overcome by employing hybrid feedback with a properly defined switching logic [2]. In particular, hybrid feedback derived from a family of synergistic potential functions can be used to globally asymptotically stabilize compact sets using gradient descent and a hysteretic switching mechanism [3], [4]. Hybrid feedback has been employed to achieve global asymptotic stability of compact sets for planar orientation control [5], [6], reduced orientation control [7], spatial orientation control [8], [9], tracking of underwater vehicles [10] and for more general compact manifolds [11].

This project has received funding from the European Research Council (ERC) under the European Union's Horizon 2020 research and innovation programme, through the ERC Advanced Grant 101017697-CRÈME. The work is also supported by the Research Council of Norway through the Centres of Excellence funding scheme, project No. 223254 – NTNU AMOS.

♯ E.A. Basso and H.M Schmidt-Didlaukies contributed equally to this work and should be considered co-first authors

The authors are with the Centre for Autonomous Marine Operations and Systems (NTNU AMOS), Norwegian University of Science and Technology, NO-7491 Trondheim, Norway {erlend.a.basso,henrik.schmidt,kristin.y.pettersen,asgeir.sorensen}@ntnu.no

While employing hybrid feedback to overcome topological obstructions on compact manifolds has been extensively studied through simulations in the idealized case where the model structure and the model parameters are assumed to be known, little attention has been paid to the more practical case involving parametric modeling uncertainties. In [12], a global exponential tracking controller with integral action is derived for the orientation control of a spatial rigid body subject to a matched and constant disturbance. Hybrid feedback using synergistic potential functions was extended to the case where the original control system is subject to matched uncertainties in [13]. However, when applying this approach to mechanical systems, the switching mechanism is not independent of the system velocities. Moreover, the approach does not permit estimation of the inertia matrix parameters.

Some of the first adaptive control laws proposed for underwater vehicles can be found in [14] and [15], where Euler angle representations were utilized for the vehicle orientation. The first quaternion-based control laws for underwater vehicles were introduced in [16], while adaptive and quaternion-based control approaches for underwater vehicles can be found in [17] and [18]. None of the aforementioned quaternion-based approaches achieve global asymptotic stability results, since they only stabilize one of the equilibrium points corresponding to the desired orientation. Adaptive backstepping designs for tracking control of ships were introduced in [19], [20], and [21]. However, none of these methods permit estimation of the inertia matrix parameters, and all of them lift the vehicle orientation from the circle to the field of real numbers, which leads to unwinding problems.

To the best of the authors' knowledge, experimental validations of globally stabilizing hybrid control laws for surface and underwater vehicles are virtually nonexistent in the existing literature. A combined hybrid observer/controller for dynamic positioning of a marine surface vehicle with global exponential stability properties was proposed in [22]. However, this result was achieved by a priori assuming that the angular velocity is bounded and by lifting the vehicle orientation from the circle to the field of real numbers, which leads to unwinding problems.

The main contribution of this paper is the development of an adaptive hybrid feedback controller for global asymptotic tracking of a hybrid reference system for marine vehicles subject to parametric uncertainties. In contrast to backstepping-based hybrid adaptive control [13], the proposed approach

permits estimation of the inertia matrix, and the switching mechanism is independent of the system velocities. As our approach is based on traditional Euler-Lagrange system models, the adaptive hybrid control law is applicable to other mechanical systems as well. In particular, it can easily be extended to robot manipulators or, more generally, vehicle-manipulator systems. The hybrid reference system is constructed from a parametrized loop and a speed assignment for the motion along the loop. The main benefit of this formulation is that it decouples the design of the path from the motion along the path, allowing us to globally asymptotically track a given parametrized loop at a desired and time-varying speed. The proposed reference system can be considered an adaptation of the maneuvering problem [23], [24] to a hybrid dynamical systems setting. Preliminary results were presented in [25], and in this paper we extend the hybrid feedback control law from surface vehicles to a more general class of Euler-Lagrange systems on $\mathrm{SE}(2)$ or $\mathrm{SE}(3)$ satisfying a set of general conditions on the switching mechanism and the potential functions. Moreover, we show that the potential functions and switching mechanisms introduced in [25] and [26] satisfy these conditions, and these potential functions and switching mechanisms are subsequently employed to design hybrid adaptive control laws for surface and underwater vehicles, respectively. Finally, we validate the theoretical developments for surface and underwater vehicle applications through experiments.

This paper is organized as follows. Section II introduces the notation, terminology and mathematical preliminaries that will be used throughout this paper. Then, Section III presents kinematic and dynamic models of marine vehicles, a hybrid reference system based on a parametrized loop and the problem statement. The hybrid control law developed in Section IV is based on a set of potential functions and a hysteretic switching mechanism. In Section V, we construct potential functions and switching mechanisms to overcome the topological obstructions of $\mathrm{SE}(2)$ and $\mathrm{SE}(3)$. Moreover, we show that the aforementioned potential functions and switching mechanisms satisfy the assumptions in Section IV. In Section VI, we present the results of three experiments conducted on marine surface and underwater vehicles, and then, Section VII concludes the paper.

II. Preliminaries

A. Notation

We denote the set of nonnegative integers by $\mathbb{Z}_{\geq 0}$, the field of real (complex) numbers is denoted $\mathbb{R}$ ($\mathbb{C}$), the real (complex) space of dimension n is denoted $\mathbb{R}^n$ ($\mathbb{C}^n$), and $\mathbb{R}^{n\times n}$ ($\mathbb{C}^{n\times n}$) is the space of $n \times n$ matrices with real (complex) entries. The Euclidean inner product in $\mathbb{R}^n$ is written $\langle x, y\rangle$ and the Euclidean norm is denoted $|x| = \langle x, x\rangle^{1/2}$. The entry of a matrix $a \in \mathbb{R}^{n\times n}$ corresponding to the ith row and jth column is denoted a_{ij}. The unit n-sphere embedded in $\mathbb{R}^{n+1}$ is given by $\mathbb{S}^n = \{x \in \mathbb{R}^{n+1} : |x| = 1\}$. Furthermore, for a set $\mathcal{S} \subset \mathcal{X} \coloneqq \mathcal{X}_1 \times \mathcal{X}_2$, the projection of $\mathcal{S}$ onto the set $\mathcal{X}_1$ is defined by $\pi_{\mathcal{X}_1}(\mathcal{S}) \coloneqq \{x_1 \in \mathcal{X}_1 : (x_1, x_2) \in \mathcal{S} \text{ for some } x_2 \in \mathcal{X}_2\}$. The range (or equivalently, the image) of a mapping $f : \mathbb{R}^m \to \mathbb{R}^n$ is defined as $\operatorname{rge} f = \{y \in \mathbb{R}^n \colon \exists x \in \mathbb{R}^m \text{ such that } y = f(x)\}$. We say that a mapping $f : \mathbb{R}^m \to \mathbb{R}^n$ is of class C^r for a nonnegative integer r if f is r-times continuously differentiable. For a C^k mapping $f : \mathbb{R} \to \mathbb{R}^n$, we denote the derivatives by $f', f'', f^{(3)}, \ldots, f^{(k)}$, with $f^{(0)} = f$. Finally, a function $V : \mathcal{Y} \to \mathbb{R}$, where $\mathcal{Y} \subset \mathbb{R}^n$, is proper if the preimage of any compact set $K \subset \mathbb{R}$ under V is compact.

B. Matrix Lie Groups

Lie groups are smooth manifolds that are also groups in which multiplication and inversion are smooth mappings. A matrix Lie group G is a closed subgroup of the general linear group $\mathrm{GL}(n) = \{g \in \mathbb{R}^{n\times n} : \det g \neq 0\}$. The identity element is denoted $e \in \mathrm{G}$. The Lie algebra of a matrix Lie group G is denoted $\mathfrak{g}$, and is defined as $\mathfrak{g} \coloneqq \{a \in \mathbb{R}^{n\times n} : t \in \mathbb{R} \implies \exp(at) \in \mathrm{G}\}$, where $\exp : \mathbb{R}^{n\times n} \to \mathrm{GL}(n)$ is the matrix exponential. Note that there is no loss of generality in assuming that g is real-valued, since $\mathrm{GL}(n, \mathbb{C}) = \{g \in \mathbb{C}^{n\times n} : \det g \neq 0\}$ is isomorphic to a Lie subgroup of $\mathrm{GL}(2n)$. The Lie algebra $\mathfrak{g}$ is a real vector space with dimension equal to the dimension of G as a manifold. Therefore, there exists an isomorphism $(\cdot)^\wedge \colon \mathbb{R}^k \to \mathfrak{g}$ with inverse $(\cdot)^\vee \colon \mathfrak{g} \to \mathbb{R}^k$, where k denotes the dimension of G. For $g \in \mathrm{G}, \xi \in \mathbb{R}^k$ and $\zeta \in \mathbb{R}^k$, we define the adjoint mappings $\mathrm{Ad} : \mathrm{G} \times \mathbb{R}^k \to \mathbb{R}^k$ and $\mathrm{ad} : \mathbb{R}^k \times \mathbb{R}^k \to \mathbb{R}^k$ by $\mathrm{Ad}_g \xi \coloneqq \left(g\xi^\wedge g^{-1}\right)^\vee$ and $\mathrm{ad}_\xi \zeta \coloneqq \left(\xi^\wedge\zeta^\wedge - \zeta^\wedge\xi^\wedge\right)^\vee$, respectively. For each $\xi \in \mathbb{R}^k$, we define a left-invariant vector field $X_\xi(g) = g\xi^\wedge$ on G with $g \in \mathrm{G}$. The Lie derivative of a continuously differentiable function $V \colon \mathrm{G} \to \mathbb{R}$ along the vector field X_ξ can be written as $\langle\!\langle \mathrm{D}V(g), X_\xi(g)\rangle\!\rangle$, where $\langle\!\langle a, b\rangle\!\rangle \coloneqq \operatorname{tr}\left(a^\mathsf{T} b\right)$ is the Frobenius inner product and

$$\mathrm{D}V(a) = \begin{pmatrix} \frac{\partial V}{\partial a_{11}} & \cdots & \frac{\partial V}{\partial a_{1j}} \\ \vdots & \ddots & \vdots \\ \frac{\partial V}{\partial a_{i1}} & \cdots & \frac{\partial V}{\partial a_{ij}} \end{pmatrix}.$$

The Lie derivative can be rewritten using the Euclidean inner product by defining the mapping $\mathrm{d}V : \mathrm{G} \to \mathbb{R}^k$ by $\langle \mathrm{d}V(g), \xi\rangle \coloneqq \langle\!\langle \mathrm{D}V(g), X_\xi(g)\rangle\!\rangle$. Finally, the bilinear map $\nabla^M \colon \mathbb{R}^k \times \mathbb{R}^k \to \mathbb{R}^k$ induced by the inertia matrix M is defined by [27]

$$\nabla^M_\nu \eta \coloneqq \tfrac{1}{2}\,\mathrm{ad}_\nu\,\eta - \tfrac{1}{2}M^{-1}[\mathrm{ad}^\mathsf{T}_\nu\, M\eta + \mathrm{ad}^\mathsf{T}_\eta\, M\nu]. \tag{1}$$

Observe that $M\nabla^M_\nu\nu = -\,\mathrm{ad}^\mathsf{T}_\nu\, M\nu$. In this work, we consider matrix Lie groups of the form $\mathrm{G} = \mathbb{R}^m \rtimes \mathrm{H}$, where $\rtimes$ denotes the semidirect product, $\mathbb{R}^m$ is a normal subgroup and H is a subgroup [28]. In particular, we will consider the subgroups $\mathrm{SO}(m) = \{R \in \mathbb{R}^{m\times m} \colon R^\mathsf{T}R = RR^\mathsf{T} = e, \det R = 1\}$ and $\mathrm{SU}(2) = \left\{\begin{pmatrix} \alpha & -\bar{\beta} \\ \beta & \bar{\alpha} \end{pmatrix} : \alpha, \beta \in \mathbb{C}, |\alpha|^2 + |\beta|^2 = 1\right\}$.

III. Modeling and Problem Statement

This section begins by presenting kinematic and dynamic models of marine vehicles. Then, we derive a hybrid reference system generating continuous and bounded configuration, velocity and acceleration references from a parametrized loop. Moreover, the motion along the path can be independently controlled by specifying a desired speed, which takes values within a compact interval. Finally, we derive the error system and formulate the problem statement.

A. Models for Surface and Underwater Marine Vehicles

The configuration of a marine vehicle can be identified with a matrix Lie group $\mathrm{G} \subset \mathbb{R}^{n\times n}$ of dimension $k \leq 6$. Let $g \in \mathrm{G}$ denote the configuration and $\nu = (v, \omega) \in \mathbb{R}^k$ denote the body velocity, where v and ω denote the linear and angular velocities of the vehicle. Using the Lie group structure of the configuration space, the equations of motion for fully actuated marine vehicles are given by

$$\dot{g} = g\nu^{\wedge}, \tag{2a}$$
$$M\dot{\nu} - \mathrm{ad}_{\nu}^{\mathsf{T}} M\nu = d(\nu) + f(g) + \tau, \tag{2b}$$

where $M \in \mathbb{R}^{k\times k}$ is the inertia matrix, including hydrodynamic added mass, $\mathrm{ad}_{\nu}^{\mathsf{T}} M\nu$ describes Coriolis and centrifugal forces, the function $d : \mathbb{R}^k \to \mathbb{R}^k$ describes dissipative forces, $f : \mathrm{G} \to \mathbb{R}^k$ contains potential forces and disturbances, and $\tau \in \mathbb{R}^k$ is the control force. Observe that the dynamic equation (2b) coincides with the dynamic equations of motion in [29, Ch. 7,8] and [30, Ch. 2] by identifying $C(\nu)\bar{\nu} := -\mathrm{ad}_{\bar{\nu}}^{\mathsf{T}} M\nu$.

B. Hybrid Reference System

We construct a hybrid reference trajectory $g_d : \mathbb{R}_{\geq 0} \times \mathbb{Z}_{\geq 0} \to \mathrm{G}$ by composing a path $\gamma : [0, 1] \to \mathrm{G}$ with a time scaling $s : \mathbb{R}_{\geq 0} \times \mathbb{Z}_{\geq 0} \to [0, 1]$, i.e. $g_d(t, j) = \gamma(s(t, j))$. A key advantage of this formulation is that it decouples the geometric path from the desired motion along the path.

Definition 1: Let $\mathcal{I} = [0, 1]$, $\mathrm{H}_2 = \mathrm{SO}(2)$, $\mathrm{H}_3 = \mathrm{SU}(2)$ and $m \in \{2, 3\}$. The parametric C^r-path $\gamma\colon \mathcal{I} \to \mathrm{G} := \mathbb{R}^m \rtimes \mathrm{H}_m$ defined by

$$\gamma(s) := (\gamma_1(s), \gamma_2(s)), \quad \gamma_1(s) \in \mathbb{R}^m, \gamma_2(s) \in \mathrm{H}_m, \tag{3}$$

is a C^r-loop if it satisfies

$$\gamma^{(j)}(0) = \gamma^{(j)}(1), \tag{4}$$

for all $0 \leq j \leq r$.

Given a loop γ, the motion along the loop can be controlled through a speed assignment for $\dot{s}$. In particular, by assuming that $|\gamma_1'(s)| \neq 0$ for all $s \in \mathcal{I}$, the desired speed of the vehicle can be controlled through the following speed assignment [23]

$$\dot{s} = \varrho(s, u_d) := \frac{u_d}{|\gamma_1'(s)|}, \tag{5}$$

where $u_d \in \mathbb{R}$ is a desired input speed. To ensure continuity of the velocity and acceleration references, the desired speed can be obtained from the following set-valued second-order low-pass filter with natural frequency $\omega_n > 0$ and damping factor $\zeta_f > 0$

$$\ddot{u}_d \in \mathcal{U}(u_d, \dot{u}_d) := \omega_n^2[0, c] - 2\zeta_f\omega_n\dot{u}_d - \omega_n^2 u_d, \tag{6}$$

where the interval $[0, c]$, with $c > 0$, contains the values of the commanded input speed μ.

Let $\Omega_1, \Omega_2 \subset \mathbb{R}$ be compact. The Lie group structure of the desired path γ leads to the following hybrid reference system:

$$\mathscr{R}:\begin{cases} \left.\begin{aligned} \dot{s} &= \varrho(s, u_d) \\ \dot{u}_d &= a_d \\ \dot{a}_d &\in \mathcal{U}(u_d, a_d) \end{aligned}\right\} & (s, u_d, a_d) \in \mathcal{I} \times \Omega_1 \times \Omega_2 \\ s^+ = 0 & (s, u_d, a_d) \in \{1\} \times \Omega_1 \times \Omega_2 \\ g_d = \gamma(s) & \\ \nu_d = \kappa(s)\varrho(s, u_d) & \\ \alpha_d = f_d(s, u_d, a_d) & \end{cases}$$

where $\kappa(s) = (\gamma(s)^{-1}\gamma'(s))^{\vee}$ is the desired tangent vector expressed in the desired frame and the mapping $f_d\colon \mathcal{I} \times \Omega_1 \times \Omega_2 \to \mathbb{R}^k$ is given by

$$f_d(\cdot) = \kappa(s)\left(\frac{\partial \varrho}{\partial s}\varrho(s, u_d) + \frac{\partial \varrho}{\partial u_d}a_d\right) + \kappa'(s)\varrho(s, u_d). \tag{7}$$

Conceptually, $\mathscr{R}$ can be considered as a hybrid system with the commanded speed $\mu \in [0, c]$ as the input, and

$$y := (g_d, \nu_d, \alpha_d) = (\gamma(s), \kappa(s)\varrho(s, u_d), f_d(s, u_d, a_d)), \tag{8}$$

as the output, where $g_d \in \operatorname{rge}\gamma$, $\nu_d \in \mathbb{R}^k$ and $\alpha_d \in \mathbb{R}^k$ are the desired configuration, velocity and acceleration references, respectively. We remark that the speed assignment for $\dot{s}$ in (5) ensures that the norm of the desired linear velocity v_d is equal to the desired speed u_d. Note that if γ is a C^2-loop, then it follows from $\gamma^{(j)}(0) = \gamma^{(j)}(1)$ for all $0 \leq j \leq 2$ and continuity of u_d, a_d that the output map $y = (g_d, \nu_d, \alpha_d)$ is continuous. We remark that for practical purposes, only a compact path is required. This, in turn, removes the switching component of the reference system. However, the loop assumption helps ensure that every maximal solution is complete.

C. Error System and Problem Statement

The error dynamics are obtained by considering the continuous and invertible transformation $(g, \nu, r) \mapsto (g_e, \nu_e, r)$, using the natural (and left-invariant) error defined by [27]

$$g_e := g_d^{-1}g, \tag{9}$$
$$\nu_e := \nu - \mathrm{Ad}_{g_e^{-1}}\nu_d. \tag{10}$$

We observe that g_e expresses the configuration of the vehicle-fixed frame with respect to the desired vehicle-fixed frame, while the term $\nu_r := \mathrm{Ad}_{g_e^{-1}}\nu_d$ can be interpreted as ν_d expressed in the vehicle-fixed frame. Moreover, the time derivative of ν_r satisfies

$$\dot{\nu}_r = \mathrm{Ad}_{g_e^{-1}}\alpha_d - \mathrm{ad}_{\nu_e}\mathrm{Ad}_{g_e^{-1}}\nu_d. \tag{11}$$

The error dynamics can now be stated as

$$\mathscr{N}:\begin{cases} \left.\begin{aligned} \dot{g}_e &= g_e\nu_e^{\wedge} \\ \dot{\nu}_e &= f_e(g_e, \nu_e, s, u_d, a_d, \tau) \\ \dot{s} &= \varrho(s, u_d) \\ \dot{u}_d &= a_d \\ \dot{a}_d &\in \mathcal{U}(u_d, a_d) \end{aligned}\right\} & (g_e, \nu_e, s, u_d, a_d) \in \widehat{\mathcal{C}} \\ s^+ = 0 & (g_e, \nu_e, s, u_d, a_d) \in \widehat{\mathcal{D}} \end{cases}$$

where $\widehat{\mathcal{C}} = \mathrm{G}\times\mathbb{R}^k\times\mathcal{I}\times\Omega_1\times\Omega_2$, $\widehat{\mathcal{D}} = \mathrm{G}\times\mathbb{R}^k\times\{1\}\times\Omega_1\times\Omega_2$ and the mapping $f_e\colon \mathrm{G}\times\mathbb{R}^k\times\mathcal{I}\times\Omega_1\times\Omega_2\times\mathbb{R}^k\to\mathbb{R}^k$ is given by

$$\begin{aligned} f_e(\cdot) \coloneqq M^{-1}(\tau - M\nabla^M_\nu\nu + d(\nu) + f(g)) \\ - \mathrm{Ad}_{g_e^{-1}} f_d(s,u_d,a_d) + \mathrm{ad}_{\nu_e}\mathrm{Ad}_{g_e^{-1}}\kappa(s)\varrho(s,u_d). \end{aligned} \tag{12}$$

We remark that the matrix representation of the adjoint maps Ad and ad are provided in Section VI for the Lie groups $\mathrm{SE}(2)$ and $\mathrm{SE}(3)$ and their Lie algebras $\mathfrak{se}(2)$ and $\mathfrak{se}(3)$.

Lemma 1: The hybrid system $\mathscr{N}$ satisfies the hybrid basic conditions [31, Assumption 6.5].

Proof: The flow and jump sets $\widehat{\mathcal{C}}$ and $\widehat{\mathcal{D}}$ are closed since Ω_1 and Ω_2 are closed. Moreover, the jump map is single-valued and continuous. The flow map is single-valued and continuous for every state except a_d. However, since the set-valued mapping $\mathcal{U}$ is outer semicontinuous, convex and locally bounded, the flow map is outer semicontinuous, convex-valued and locally bounded. ■

Problem Statement: For a given C^2-loop γ, the speed assignment ϱ defined in (5) for $\dot{s}$ and a compact set $\mathcal{A}^\circ\subset\mathrm{G}$, design a hybrid feedback control law with output $\tau\in\mathbb{R}^k$ such that every solution to $\mathscr{N}$ is bounded and converges to the compact set

$$\mathcal{B} = \{(g_e,\nu_e,s,u_d,a_d) : g_e\in\mathcal{A}^\circ, \nu_e = 0\}, \tag{13}$$

for the system $\mathscr{N}$ under parametric uncertainties.

IV. Hybrid Control Design

In this section, we propose an adaptive hybrid feedback control law for the system $\mathscr{N}$. The control law is derived from a set of potential functions and a hysteretic switching mechanism encoded by the flow and jump sets and the jump map. The hybrid controller is based on the following assumption.

Assumption 1: Given a 5-tuple $(\mathcal{A},\mathcal{C},\mathcal{D},\mathcal{G},V)$, where $V:\mathcal{O}\to\mathbb{R}$ is defined by $(g,q)\mapsto V(g,q) = V_q(g)$, where $q\in\mathcal{Q}$ is a logic variable, $\mathcal{Q}\subset\mathbb{R}$ is a finite set and $\mathcal{O}$ is an open set containing $\mathcal{C}$

(A1) $\mathcal{A}\subset\mathcal{C}$ is a compact set and $\pi_{\mathrm{G}}(\mathcal{A}) = \mathcal{A}^\circ$;

(A2) $\mathcal{C}$ and $\mathcal{D}$ are closed subsets of $\mathrm{G}\times\mathcal{Q}$ such that $\mathcal{C}\cup\mathcal{D} = \mathrm{G}\times\mathcal{Q}$ and $\pi_{\mathrm{G}}(\mathcal{C}) = \mathrm{G}$;

(A3) The set-valued mapping $\mathcal{G}:\mathcal{D}\rightrightarrows\mathcal{Q}$ is nonempty for all $(g,q)\in\mathcal{D}$ and outer semicontinuous and locally bounded relative to $\mathcal{D}$;

(A4) for every $(g,q)\in\mathcal{C}\cap\mathcal{D}$, it holds that $(g,w)\in\mathcal{C}\setminus\mathcal{D}$ for each $w\in\mathcal{G}(g,q)$;

(A5) there exists $N\in\mathbb{Z}_{\geq 1}$ such that for every $(g,q)\in\mathcal{D}$, it holds that $(g,w)\in\mathcal{C}\setminus\mathcal{D}$ for each $(g,w)\in\overline{\mathcal{G}}^K(g,q)$, where $1\leq K\leq N$, $\overline{\mathcal{G}}(g,q) = \{g\}\times\mathcal{G}(g,q)$ and $\overline{\mathcal{G}}^K \coloneqq \underbrace{\overline{\mathcal{G}}\circ\overline{\mathcal{G}}\circ\cdots\circ\overline{\mathcal{G}}}_{K\text{times}}$;

(A6) V is continuously differentiable on $\mathcal{O}$ and is proper and positive definite on $\mathcal{C}$ with respect to $\mathcal{A}$;

(A7) for all $(g,q)\in\mathcal{C}\cap\mathcal{D}$ and each $w\in\mathcal{G}(g,q)$

$$V_w(g) - V_q(g)\leq 0; \tag{14}$$

(A8) for all $(g,q)\in\mathcal{C}$, $\mathrm{d}V_q(g) = 0$ if and only if $(g,q)\in\mathcal{A}$.

Assumption 1 guarantees that the switching is hysteretic, the hybrid control law satisfies the hybrid basic conditions and is required to ensure that every solution to $\mathscr{N}$ converges to $\mathcal{B}$.

We remark that the conditions of Assumption 1 are different from the conditions for synergistic control [32, Definition 7.3]. First, they do not enforce a strict decrease in V across jumps. Second, they are not restricted to a switching mechanism based on the value of the potential functions V_q. Finally, they permit each potential function V_q to be defined locally, i.e., having a domain that is a strict subset of G.

To establish convergence to the set $\mathcal{B}$ when the model parameters are unknown, we define the modified reference velocity $\nu_m\in\mathbb{R}^k$ and the corresponding reference velocity error $\zeta\coloneqq\nu_m-\nu_r$ through the differential equation

$$\Lambda[\dot{\zeta} + \nabla^\Lambda_\nu\zeta] = -\mathrm{d}V_q(g_e) - \vartheta_q(\zeta), \tag{15}$$

where $\vartheta:\mathbb{R}^k\times\mathcal{Q}\to\mathbb{R}^k$ satisfies $\vartheta_q(\zeta)^\mathsf{T}\zeta>0$ for each $q\in\mathcal{Q}$ and for all $\zeta\neq 0$. We remark that ϑ can be chosen independent of q and that the term $\Lambda\nabla^\Lambda_\nu\zeta$ is optional. The latter is because $\langle\zeta,\Lambda\nabla^\Lambda_\xi\zeta\rangle = 0$ for any $\xi\in\mathbb{R}^k$, which entails that any velocity can be used in place of ν in the bilinear map ∇^Λ. The velocity error is now redefined as

$$\xi\coloneqq\nu-\nu_m = \nu_e-\zeta. \tag{16}$$

Since $\zeta=0$ implies $\xi=\nu_e$, the velocity tracking control objective $\nu_e=0$ is accomplished when $(\xi,\zeta)=0$. In practice, this type of velocity error may be advantageous when the configuration error encoded by $\mathrm{d}V$ is significant while the velocity error ν_e is zero.

Before delving into the proposed adaptive controller, we begin by presenting the non-adaptive version. Given a 5-tuple $(\mathcal{A},\mathcal{C},\mathcal{D},\mathcal{G},V)$ satisfying Assumption 1 and if the model parameters in (2) are known, we propose the following hybrid control law

$$\begin{cases} \dot{\zeta} = -\nabla^\Lambda_\nu\zeta - \Lambda^{-1}\big(\mathrm{d}V_q(g_e) + \vartheta_q(\zeta)\big), & (g_e,q)\in\mathcal{C} \\ q^+\in\mathcal{G}(g_e,q), & (g_e,q)\in\mathcal{D} \\ \tau = M[\dot{\nu}_m + \nabla^M_\nu\nu_m] - d(\nu) \\ \quad - f(g) - \mathrm{d}V_q(g_e) - \varphi_q(\xi). \end{cases} \tag{17}$$

Observe that the feedback control law (17) comprises a proportional action $\mathrm{d}V$ and a derivative action φ, where $\varphi\colon\mathbb{R}^k\times\mathcal{Q}\to\mathbb{R}^k$ is such that $\varphi_q(\xi)^\mathsf{T}\xi>0$, for each $q\in\mathcal{Q}$, and for all $\xi\neq 0$. In other words, the control law (17) is essentially a PD+ control law [33] with desired velocity ν_m and hysteretic switching. We note that the derivative action can be chosen independently of the logic variable q. However, the proportional action can only be chosen independently of q provided that the configuration space is globally diffeomorphic to Euclidean space.

To make the control law (17) adaptive, we make the following assumption on the unknown model parameters.

Assumption 2: There exists a known matrix-valued function of available data $\Phi\colon\mathrm{G}\times\mathbb{R}^k\times\mathbb{R}^k\times\mathcal{I}\times\Omega_1\times\Omega_2\to\mathbb{R}^{k\times l}$ and a vector of unknown model parameters $\theta\in\mathbb{R}^l$ with known lower and upper bounds $\underline{\theta}$ and $\overline{\theta}$ such that

$$M[\dot{\nu}_m+\nabla^M_\nu\nu_m] - d(\nu) - f(g) = \Phi(g_e,\zeta,\xi,s,u_d,a_d)\theta, \tag{18}$$

for all $(g_e, \zeta, \xi, s, u_d, a_d) \in \mathrm{G} \times \mathbb{R}^k \times \mathbb{R}^k \times \mathcal{I} \times \Omega_1 \times \Omega_2$. The boundedness assumption on the parameters is justified by the fact that the parameters represent real physical quantities that we often have rough estimates of in practice. Assumption 2 implies that the parameters are contained in the convex set

$$\mathcal{P} \coloneqq \{\theta \in \mathbb{R}^l : \underline{\theta} \leq \theta \leq \overline{\theta}\}. \tag{19}$$

Define the extended tangent cone to $\mathcal{P}$ by

$$\begin{aligned} T_{\mathbb{R},\mathcal{P}}(\theta) \coloneqq T_{\mathbb{R},[\underline{\theta}_1,\overline{\theta}_1]}(\theta_1) \times T_{\mathbb{R},[\underline{\theta}_2,\overline{\theta}_2]}(\theta_2) \times \cdots \\ \times T_{\mathbb{R},[\underline{\theta}_l,\overline{\theta}_l]}(\theta_l), \end{aligned} \tag{20}$$

where the extended tangent cone to each interval is given by

$$T_{\mathbb{R},[\underline{\theta}_i,\overline{\theta}_i]}(\theta_i) \coloneqq \begin{cases} [0,\infty) & \text{if } \theta_i \leq \underline{\theta}_i \\ (-\infty,\infty) & \text{if } \theta_i \in (\underline{\theta}_i,\overline{\theta}_i) \\ (-\infty,0] & \text{if } \theta_i \geq \overline{\theta}_i \end{cases} \tag{21}$$

Let $\theta_a \in \mathbb{R}^l$ denote the estimate of θ and define the convex set

$$\mathcal{P}_\epsilon \coloneqq \{\theta_a \in \mathbb{R}^l : \underline{\theta} - \epsilon \leq \theta_a \leq \overline{\theta} + \epsilon\}, \tag{22}$$

where $\epsilon = (\epsilon_1, \ldots, \epsilon_l) \in \mathbb{R}^l$, defines boundary layers of length $\epsilon_i > 0$ around each interval in (19). The goal is to enforce $\theta_a \in \mathcal{P}_\epsilon$ through the adaptive update law. To this end, we define the projection operator $\mathrm{Proj}\colon \mathbb{R}^l \times \mathcal{P}_\epsilon \to \mathbb{R}^l$ by [34]

$$\mathrm{Proj}(\chi, \theta_a) \coloneqq \begin{cases} \chi, & \text{if } \chi \in T_{\mathbb{R},\Omega}(\theta_a) \\ (1 - h(\theta_a))\chi & \text{if } \chi \notin T_{\mathbb{R},\Omega}(\theta_a) \end{cases} \tag{23}$$

where the components of $h(\theta_a)$ are given by

$$h_i(\theta_{a,i}) = \begin{cases} 0, & \text{if } \theta_{a,i} \in (\underline{\theta}_i,\overline{\theta}_i) \\ \min\{1, \frac{\underline{\theta}_i - \theta_{a,i}}{\epsilon_i}\}, & \text{if } \theta_{a,i} \leq \underline{\theta}_i \\ \min\{1, \frac{\theta_{a,i} - \overline{\theta}_i}{\epsilon_i}\}, & \text{if } \theta_{a,i} \geq \overline{\theta}_i \end{cases} \tag{24}$$

The following lemma can be found in [34, Lemma E.1].

Lemma 2: The projection operator (23) satisfies

(P1) The mapping $\mathrm{Proj}\colon \mathbb{R}^l \times \mathcal{P}_\epsilon \to \mathbb{R}^l$ is Lipschitz continuous in χ and θ_a.

(P2) The differential equation

$$\dot{\theta}_a = \mathrm{Proj}(\chi, \theta_a), \quad \theta_a(t_0) \in \mathcal{P}_\epsilon, \tag{25}$$

satisfies $\theta_a \in \mathcal{P}_\epsilon$ for all $t \geq t_0$.

(P3) Let $\theta_e = \theta - \theta_a$ denote the estimation error, then

$$-\langle \theta_e, \Gamma^{-1}\mathrm{Proj}(\chi, \theta_a)\rangle \leq -\langle \theta_e, \Gamma^{-1}\chi\rangle, \tag{26}$$

for all $\theta_a \in \mathcal{P}_\epsilon$ and $\theta \in \mathcal{P}$.

Using (18) and the projection operator defined in (23), we define an adaptive version of (17) by

$$\left.\begin{aligned} \dot{\zeta} &= -\nabla_\nu^\Lambda \zeta - \Lambda^{-1}\big(\mathrm{d}V_q(g_e) + \vartheta_q(\zeta)\big) \\ \dot{\theta}_a &= \mathrm{Proj}(-\Gamma\Phi(g_e, \zeta, \xi, s, u_d, a_d)^\mathsf{T}\xi, \theta_a) \end{aligned}\right\} (g_e, q) \in \mathcal{C}$$
$$q^+ \in \mathcal{G}(g_e, q) \qquad (g_e, q) \in \mathcal{D} \tag{27}$$
$$\tau = \Phi(g_e, \zeta, \xi, s, u_d, a_d)\theta_a - \mathrm{d}V_q(g_e) - \varphi_q(\xi).$$

By defining $x \coloneqq (g_e, \xi, s, u_d, a_d, \zeta, \theta_a, q) \in \mathcal{X}$ and the extended state space

$$\mathcal{X} \coloneqq \mathrm{G} \times \mathbb{R}^k \times \mathcal{I} \times \Omega_1 \times \Omega_2 \times \mathbb{R}^k \times \mathcal{P}_\epsilon \times \mathcal{Q}, \tag{28}$$

the adaptive hybrid control law (27) applied to the hybrid system $\mathscr{N}$ leads to the hybrid closed-loop system

$$\mathscr{H}\colon \begin{cases} \left.\begin{aligned} \dot{g}_e &= g_e(\xi + \zeta)^\wedge \\ \dot{\xi} &= \tilde{f}(x) \\ \dot{s} &= \varrho(s, u_d) \\ \dot{u}_d &= a_d \\ \dot{a}_d &\in \mathcal{U}(u_d, a_d) \\ \dot{\zeta} &= -\nabla_\nu^\Lambda \zeta - \Lambda^{-1}\big(\mathrm{d}V_q(g_e) + \vartheta_q(\zeta)\big) \\ \dot{\theta}_a &= \mathrm{Proj}(-\Gamma\Phi(g_e, \zeta, \xi, s, u_d, a_d)^\mathsf{T}\xi, \theta_a) \end{aligned}\right\} & x \in \widetilde{\mathcal{C}} \\ (q^+, s^+) \in \widetilde{\mathcal{G}}(g_e, q, s) & x \in \widetilde{\mathcal{D}}, \end{cases} \tag{29}$$

where

$$\begin{aligned} \tilde{f}(x) \coloneqq -M^{-1}\Phi(g_e, \zeta, \xi, s, u_d, a_d)\theta_e - \nabla_\nu^M \xi \\ - M^{-1}(\mathrm{d}V_q(g_e) + \varphi_q(\xi)). \end{aligned} \tag{30}$$

Moreover, the jump map $\widetilde{\mathcal{G}} : \mathrm{G} \times \mathcal{Q} \times \mathcal{I} \rightrightarrows \mathcal{Q} \times \mathcal{I}$ is defined as

$$\widetilde{\mathcal{G}}(g_e, q, s) \coloneqq \begin{cases} (\mathcal{G}(g_e, q), s), & (g_e, q, s) \in \mathcal{D} \times (\mathcal{I} \backslash \{1\}) \\ \{(\mathcal{G}(g_e, q), s), (q, 0)\} & (g_e, q, s) \in \mathcal{D} \times \{1\} \\ (q, 0), & (g_e, q, s) \in (\mathcal{C} \backslash \mathcal{D}) \times \{1\} \end{cases} \tag{31}$$

while the flow set $\widetilde{\mathcal{C}}$ and jump set $\widetilde{\mathcal{D}}$ are defined by

$$\widetilde{\mathcal{C}} \coloneqq \{x \in \mathcal{X} : (g_e, q) \in \mathcal{C}\}, \tag{32}$$

$$\widetilde{\mathcal{D}} \coloneqq \{x \in \mathcal{X} : (g_e, q) \in \mathcal{D}\} \cup \{x \in \mathcal{X} \colon s = 1\}. \tag{33}$$

Lemma 3: The closed-loop system $\mathscr{H}$ satisfies the hybrid basic conditions.

Proof: From Lemma 1, Assumption 1 and the definitions of the jump map, flow set and jump set, it follows that all of the assumptions in [32, Lemma 2.21] are satisfied. ■

Theorem 1: Let Assumption 2 hold. Given a 5-tuple $(\mathcal{A}, \mathcal{C}, \mathcal{D}, \mathcal{G}, V)$ satisfying Assumption 1, the compact set

$$\mathcal{A}_1 = \{x \in \mathcal{X} : (g_e, q) \in \mathcal{A}, \xi = 0, \zeta = 0, \theta_a = \theta\}, \tag{34}$$

is uniformly globally stable for the system $\mathscr{H}$ and every solution to $\mathscr{H}$ converges to

$$\begin{aligned} \mathcal{A}_2 = \{x \in \mathcal{X} : (g_e, q) \in \mathcal{A}, \xi = 0, \zeta = 0, \\ \Phi(g_e, 0, 0, s, u_d, a_d)\theta_e = 0\}. \end{aligned} \tag{35}$$

Proof: Let $\breve{\mathscr{H}}$ denote the hybrid system $\mathscr{H}$ with each jump set $\widetilde{\mathcal{D}}$ replaced by $\breve{\mathcal{D}} = \{x \in \mathcal{X} : (g_e, q) \in \mathcal{C} \cap \mathcal{D}\} \cup \{x \in \mathcal{X} \colon s = 1\}$ and consider the continuously differentiable function

$$\begin{aligned} W(g_e, q, \xi, \zeta, \theta_a) = V_q(g_e) + \frac{1}{2}\langle \xi, M\xi\rangle \\ + \frac{1}{2}\langle \zeta, \Lambda\zeta\rangle + \frac{1}{2}\langle \theta_e, \Gamma^{-1}\theta_e\rangle. \end{aligned} \tag{36}$$

For all $x \in \widetilde{\mathcal{C}}$, the change in W along the solutions of $\breve{\mathscr{H}}$ is

$$\begin{aligned} &\langle \mathrm{d}V_q(g_e), \nu_e \rangle + \langle \zeta, -\mathrm{d}V_q(g_e) - \vartheta_q(\zeta) \rangle \\ &+ \langle \xi, -\Phi\theta_e - M\nabla_\nu^M \xi - \mathrm{d}V_q(g_e) - \varphi_q(\xi) \rangle \\ &- \langle \theta_e, \Gamma^{-1}\mathrm{Proj}(-\Gamma\Phi^\mathsf{T}\xi, \theta_a) \rangle, \end{aligned} \tag{37}$$

which simplifies to

$$\begin{aligned} &- \langle \xi, \varphi_q(\xi) \rangle - \langle \zeta, \vartheta_q(\zeta) \rangle \\ &\quad - \langle \theta_e, \Gamma^{-1}\mathrm{Proj}(-\Gamma\Phi^\mathsf{T}\xi, \theta_a) + \Phi^\mathsf{T}\xi \rangle \\ &\leq -\langle \xi, \varphi_q(\xi) \rangle - \langle \zeta, \vartheta_q(\zeta) \rangle \\ &\leq 0, \end{aligned} \tag{38}$$

where the first inequality follows from (P3) in Lemma 2. For any $x \in \breve{\mathcal{D}}$ and $(w, m) \in \widetilde{\mathcal{G}}(g_e, q, s)$, the change in W across jumps is

$$\begin{aligned} &W(g_e, w, \xi, \zeta, \theta_a) - W(g_e, q, \xi, \zeta, \theta_a) \\ &\qquad = V_w(g_e) - V_q(g_e), \end{aligned}$$

which is clearly equal to zero when $(g_e, q, s) \in (\mathcal{C}\backslash\mathcal{D}) \times \{1\}$, i.e. when $w = q$. Otherwise, it follows from Assumption 1 that $V_w(g_e) - V_q(g_e) \leq 0$ for all $(q, w) \in \mathcal{Q} \times \pi_{\mathcal{Q}}(\widetilde{\mathcal{G}}(g_e, q, s))$. Consequently, the growth of W along solutions to $\breve{\mathscr{H}}$ is bounded by

$$u_c(x) = \begin{cases} -\langle \xi, \varphi_q(\xi) \rangle - \langle \zeta, \vartheta_q(\zeta) \rangle, & \text{if } x \in \widetilde{\mathcal{C}} \\ -\infty, & \text{otherwise} \end{cases} \tag{39}$$

$$u_d(x) = \begin{cases} 0, & \text{if } x \in \breve{\mathcal{D}} \\ -\infty, & \text{otherwise} \end{cases} \tag{40}$$

along flows and across jumps, respectively. It follows from Assumption 1 and (36) that W is proper and positive definite on $\widetilde{\mathcal{C}} \cup \breve{\mathcal{D}}$ with respect to the compact set $\mathcal{A}_1$. Hence, the proof of [31, Theorem 3.18] implies that $\mathcal{A}_1$ is uniformly globally stable for the hybrid system $\breve{\mathscr{H}}$. Observe that the system $\breve{\mathscr{H}}$ permits at most two consecutive jumps before a nonzero time of flow follows. Thus, since W is continuous, $\breve{\mathscr{H}}$ satisfies the hybrid basic conditions, and every maximal solution to $\breve{\mathscr{H}}$ is complete, it follows from [31, Corollary 8.7 (b)] that each solution to $\breve{\mathscr{H}}$ converges to the largest weakly invariant subset Ψ contained in

$$W^{-1}(r) \cap \overline{u_c^{-1}(0)}, \tag{41}$$

for some $r \in \mathbb{R}$, where

$$\overline{u_c^{-1}(0)} = \{x \in \mathcal{X} : \xi = 0, \zeta = 0, (g_e, q) \in \mathcal{C}\}. \tag{42}$$

Moreover, the closed-loop system (29) is such that $\zeta \equiv 0$ implies $\mathrm{d}V_q(g_e) \equiv 0$, and it follows from Assumption 1 that $\mathrm{d}V_q(g_e) = 0$ implies $(g_e, q) \in \mathcal{A}$. Thus, $(\xi, \zeta) \equiv 0$ implies that $\Phi(g_e, 0, 0, s, u_d, a_d)\theta_e \equiv 0$, which results in

$$\Psi \subset W^{-1}(r) \cap \overline{u_c^{-1}(0)} \subset W^{-1}(r) \cap \mathcal{A}_2 \subset \mathcal{A}_2.$$

Consequently, since every solution is complete and bounded, every solution to $\breve{\mathscr{H}}$ converges to $\mathcal{A}_2$. Solutions to $\mathscr{H}$ that are not solutions to $\breve{\mathscr{H}}$ are those with initial values x^* such that $(g_e^*, q^*) \in \mathcal{D}\backslash\mathcal{C}$. However, it follows from (A5) that such solutions exhibit $1 \leq M \leq N$ immediate and consecutive jumps from q^* to some $w \in \overline{\mathcal{G}}^M(g_e^*, q^*)$ satisfying $(g_e^*, w) \in \mathcal{C}\backslash\mathcal{D}$, after which the solutions coincide with a solution to $\mathscr{H}$. Consequently, we conclude that $\mathcal{A}_1$ is uniformly globally stable for the hybrid system $\mathscr{H}$ and that every solution to the hybrid system $\mathscr{H}$ converges to $\mathcal{A}_2$. ■

We remark that Theorem 1 implies that the problem statement is solved. Furthermore, note that uniform global asymptotic stability of the compact set

$$\widetilde{\mathcal{B}} = \{x \in \mathcal{X} : g_e \in \mathcal{A}, q \in \mathcal{R}, \zeta = 0, \xi = 0\}, \tag{43}$$

for the closed-loop system $\mathscr{H}$ implies that $\mathcal{B}$ is uniformly globally asymptotically stable for the error system $\mathscr{N}$. However, without further assumptions on the nature of the parametrized loop and commanded input speed, it is not possible to show that (27) uniformly globally asymptotically stabilizes the compact set $\widetilde{\mathcal{B}}$ for the closed-loop system $\mathscr{H}$. However, a trivial modification of the proof of Theorem 1 clearly shows that the non-adaptive hybrid control law (17) uniformly globally asymptotically stabilizes the compact set $\widetilde{\mathcal{B}}$ for the closed-loop system $\mathscr{H}$ with $\dot{\theta}_a = 0$ and $\theta_e = 0$, implying that $\mathcal{B}$ is uniformly globally asymptotically stable for the error system $\mathscr{N}$.

V. Potential Functions for Marine Vehicles

In this section we construct potential functions and derive 5-tuples $(\mathcal{A}, \mathcal{C}, \mathcal{D}, \mathcal{G}, V)$ satisfying Assumption 1 for a surface vehicle and an underwater vehicle. This 5-tuple determines the proportional control action and the switching mechanism through the potential functions V and the flow set, jump set and jump map $\mathcal{C}$, $\mathcal{D}$, $\mathcal{G}$, respectively.

A. Potential functions on $\mathrm{SE}(2)$

The configuration of a surface vehicle can be identified with the matrix Lie group $\mathrm{SE}(2) = \mathbb{R}^2 \rtimes \mathrm{SO}(2)$. An element $g = (p, R) \in \mathrm{SE}(2)$ contains the position $p = (x, y) \in \mathbb{R}^2$ and orientation $R \in \mathrm{SO}(2)$ of a vehicle-fixed frame with respect to an inertial frame.

Using the linear action of $\mathrm{SO}(2)$ on $\mathbb{R}^2$ defined by $(p, R) \mapsto Rp$, the semidirect product $\mathrm{SE}(2) = \mathbb{R}^2 \rtimes \mathrm{SO}(2)$ yields the natural error on $\mathrm{SE}(2)$

$$g_e = g_d^{-1} g = (p_e, R_e) = (R_d^\mathsf{T}(p - p_d), R_d^\mathsf{T} R). \tag{44}$$

The goal is to construct potential functions and a switching mechanism for stabilization of the configuration corresponding to the compact set

$$\mathcal{A}^\circ = \{g_e \in \mathrm{SE}(2) : p_e = 0, R_e = e\}. \tag{45}$$

To this end, we let $\delta > 0$ and define the functions $\rho_1 : D_1 \to \mathbb{R}$, $\rho_2 : D_2 \to \mathbb{R}$ and $\rho_3 : D_3 \to \mathbb{R}$, where $D_1 = D_2 := \{R \in \mathrm{SO}(2) : (\log R)^\vee \in [\delta, \pi] \cup (-\pi, -\delta]\}$ and $D_3 := \mathrm{SO}(2)$ by

$$\rho_1(R) := \begin{cases} (\log R)^\vee, & \text{if } (\log R)^\vee \in [\delta, \pi] \\ (\log R)^\vee + 2\pi, & \text{if } (\log R)^\vee \in (-\pi, -\delta] \end{cases} \tag{46a}$$

$$\rho_2(R) := \begin{cases} (\log R)^\vee, & \text{if } (\log R)^\vee \in (-\pi, -\delta] \\ (\log R)^\vee - 2\pi, & \text{if } (\log R)^\vee \in [\delta, \pi] \end{cases} \tag{46b}$$

$$\rho_3(R) := (\log R)^\vee, \tag{46c}$$

where $(\log R)^\vee = \operatorname{atan2}(R_{21}, R_{11})$ is the principal logarithm of $R \in \mathrm{SO}(2)$, which corresponds to the heading angle $\psi \in (-\pi, \pi]$ in practice. Now, for each $q \in \mathcal{Q} = \{1, 2, 3\}$, we define the potential functions $V_q : \mathcal{U}_q \times \mathbb{R}^2 \to \mathbb{R}_{\geq 0}$ by

$$V_q(g_e) \coloneqq \tfrac{1}{2} k_q \rho_q(R_e)^2 + \tfrac{1}{2} p_e^\mathsf{T} K p_e + o_q, \tag{47}$$

where $K = K^\mathsf{T} > 0$, $k_1 = k_2 = k > 0$, $k_3 > 0$, $o_1 = o_2 = o$ and $o_3 = 0$. Due to the topology of $\mathrm{SO}(2)$, at least two potential functions are required to design a globally asymptotically stable hybrid control law. However, by using three potential functions we obtain improved transient performance by encoding smaller proportional gains into the global controllers ($q \in \{1, 2\}$) relative to the local controller ($q = 3$). To this end, the role of the offsets is to enable $k_3 > k$, i.e., a larger proportional gain locally around $R_e = e$. A visualization of the rotational part of the potential functions is shown in Figure 1.

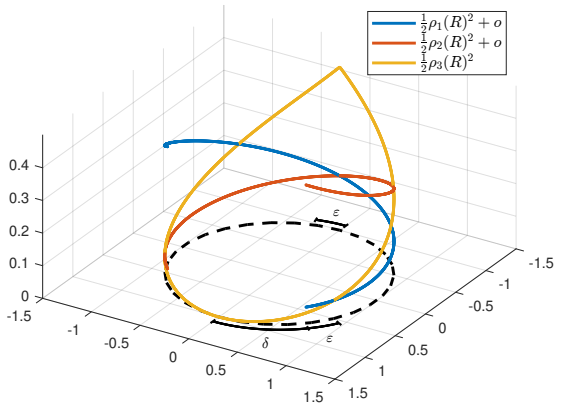

Fig. 1. The rotational part of the potential functions $\{V_q\}_{q\in\mathcal{Q}}$ with $k = \frac{1}{(2\pi)^2}$, $k_3 = \frac{4}{(2\pi)^2}$, $\delta = \frac{\pi}{4}$, $\varepsilon = \frac{\pi}{12}$, and $o = \frac{1}{2}(\delta+\varepsilon)^2(k_3 - k)$.

The switching mechanism is defined by the flow and jump sets $\mathcal{C}, \mathcal{D} \subset \mathrm{SE}(2) \times \mathcal{Q}$ and the jump map $\mathcal{G} \colon \mathcal{D} \rightrightarrows \mathcal{Q}$ associated with the potential functions $\{V_q\}_{q\in\mathcal{Q}}$. We define the flow and jump sets by

$$\mathcal{C} \coloneqq \bigcup_{q\in\mathcal{Q}} \mathcal{C}_q \times \{q\}, \tag{48a}$$

$$\mathcal{D} \coloneqq \bigcup_{q\in\mathcal{Q}} \mathcal{D}_q \times \{q\}, \tag{48b}$$

where

$$\mathcal{C}_1 \coloneqq \{g_e \in \mathrm{SE}(2) : \delta \leq \rho_1(R_e) \leq \pi + \varepsilon\}, \tag{49a}$$

$$\mathcal{C}_2 \coloneqq \{g_e \in \mathrm{SE}(2) : \delta \leq -\rho_2(R_e) \leq \pi + \varepsilon\}, \tag{49b}$$

$$\mathcal{C}_3 \coloneqq \{g_e \in \mathrm{SE}(2) : |\rho_3(R_e)| \leq \delta + \varepsilon\}. \tag{49c}$$

and

$$\begin{aligned}\mathcal{D}_1 \coloneqq &\{g_e \in \mathrm{SE}(2) \colon \pi + \varepsilon \leq \rho_1(R_e) \leq 2\pi - \delta\} \\ &\cup \{g_e \in \mathrm{SE}(2) \colon |\rho_3(R_e)| \leq \delta\}\end{aligned} \tag{50a}$$

$$\begin{aligned}\mathcal{D}_2 \coloneqq &\{g_e \in \mathrm{SE}(2) \colon \pi + \varepsilon \leq -\rho_2(R_e) \leq 2\pi - \delta\} \\ &\cup \{g_e \in \mathrm{SE}(2) \colon |\rho_3(R_e)| \leq \delta\}\end{aligned} \tag{50b}$$

$$\mathcal{D}_3 \coloneqq \{g_e \in \mathrm{SE}(2) \colon |\rho_3(R_e)| \geq \delta + \varepsilon\}. \tag{50c}$$

In (49) and (50), $\delta > 0$ determines the switching point between the local and global controllers while $\varepsilon > 0$ denotes the hysteresis half-width between the global controllers. Finally, we define the set-valued jump map for all $(g_e, q) \in \mathcal{D}$ by

$$\mathcal{G}(g_e, q) \coloneqq \{w \in \mathcal{Q} \setminus \{q\} : g_e \in \mathcal{C}_w \cap \mathcal{D}_q\}. \tag{51}$$

The following lemma provides conditions on the gains and offsets in (47), ensuring that V is nonincreasing across jumps.

Lemma 4: Let $\mathcal{A} = \mathcal{A}^\circ \times \{3\}$. If $k_3 \geq k$, $\delta + 2\varepsilon < \pi$ and

$$\tfrac{1}{2}\delta^2(k_3 - k) \leq o \leq \tfrac{1}{2}(\delta + \varepsilon)^2(k_3 - k), \tag{52}$$

then the 5-tuple $(\mathcal{A}, \mathcal{C}, \mathcal{D}, \mathcal{G}, V)$ satisfies Assumption 1.

Proof: (A1-A2) $\mathcal{A}$ is compact since it is finite, while $\mathcal{C}$ and $\mathcal{D}$ are closed subsets of $\mathrm{SE}(2) \times \mathcal{Q}$ since each ρ_q is continuous and the sublevel sets of a continuous function are closed. Moreover, $\bigcup_{q\in\mathcal{Q}} \mathcal{C}_q = \mathrm{SE}(2)$ and $\mathcal{C}_q \cup \mathcal{D}_q = \mathrm{SE}(2)$ for each $q \in \mathcal{Q}$. Hence, (A1)-(A2) hold.

(A3) Observe that $\mathcal{G}$ is locally bounded since $\operatorname{rge}\mathcal{G} = \mathcal{Q}$ is compact. Moreover, it follows from (A2) that $\mathcal{G}$ nonempty for all $(g_e, q) \in \mathcal{D}$. Since $\mathcal{G}^{-1}(w) = \bigcup_{q\neq w} (\mathcal{C}_w \cap \mathcal{D}_q) \times \{q\}$ is closed, $\operatorname{gph}\mathcal{G}^{-1} = \bigcup_{w\in\mathcal{Q}} \mathcal{G}^{-1}(w) \times \{w\}$ and the intersection of closed sets are closed, it follows from [35, Theorem 5.7 (a)] that $\mathcal{G}^{-1}$ is outer semicontinuous everywhere, and hence that $\mathcal{G}$ is outer semicontinuous everywhere.

(A4) Let $g_e \in \mathcal{C}_q \cap \mathcal{D}_q$ and $w \in \mathcal{G}(g_e, q)$. Consider the case where $q \in \{1, 2\}$. If $w = 3$, then it follows that $|\rho_3(R_e)| = \delta$, and hence that $g_e \in \mathcal{C}_3 \setminus \mathcal{D}_3$. Otherwise, $w = 3 - q$ and it follows that $|\rho_q(R_e)| = \pi + \varepsilon$, which implies that $|\rho_w(R_e)| = \pi - \varepsilon$ and hence that $g_e \in \mathcal{C}_{3-q} \setminus \mathcal{D}_{3-q}$. Finally, consider that $q = 3$. Then, $g_e \in \mathcal{C}_q \cap \mathcal{D}_q$ implies that $|\rho_3(R_e)| = \delta + \varepsilon$, which further implies that $g_e \in \mathcal{C}_w \setminus \mathcal{D}_w$.

(A5) Let $(g_e, q) \in \mathcal{D} \setminus \mathcal{C}$. Then, $g_e \in \mathcal{C}_w$ for some $w \in \mathcal{G}(g_e, q)$. Consequently, $g_e \in \mathcal{C}_w \setminus \mathcal{D}_w$ or $g_e \in \mathcal{C}_w \cap \mathcal{D}_w$. It follows from (A4) that (A5) holds with $N = 2$.

(A6) V is clearly continuously differentiable on $\mathcal{O}$ and positive definite with respect to $\mathcal{A}$. Moreover, since the function $\tilde{V} : D \to \mathbb{R}$, where $D = \bigcup_{q\in\mathcal{Q}} D_q \times \{q\}$ defined by $(R, q) \mapsto \frac{1}{2} k_q \rho_q(R)^2$ is continuous, $\pi_{\mathrm{SO}(2)}(D) = \mathrm{SO}(2)$, and $\mathrm{SO}(2)$ is compact, it follows that $\tilde{V}_q$ is proper. Additionally, the function $\check{V}_q : \mathbb{R}^2 \to \mathbb{R}$ defined by $p \mapsto \frac{1}{2} p^\mathsf{T} K p$ is radially unbounded. Consequently, $V_q(g_e) = \tilde{V}_q(R_e) + \check{V}_q(p_e)$ is a proper map.

To prove (A7), consider $g_e \in \mathcal{C}_q \cap \mathcal{D}_q$, $q \in \{1, 2\}$, $w = 3 - q$, and $0 < \varepsilon < \pi$. It follows immediately from the definitions of ρ_1 and ρ_2 that $V_{3-q}(g_e) - V_q(g_e) < 0$. When $g_e \in \mathcal{C}_q \cap \mathcal{D}_q$, $q \in \{1, 2\}$, $w = 3$, $0 < \varepsilon < \pi$ and $0 < \delta < \pi$, it holds that $\rho_3(R_e)^2 \leq \rho_q(R_e)^2$, which implies that

$$V_3(g_e) - V_q(g_e) \leq \frac{1}{2}(k_3 - k)\rho_3(R_e)^2 - o.$$

Since $k_3 - k \geq 0$ and $\rho_3(R_e)^2 \leq \delta^2$, the lower bound $o \geq \frac{1}{2}(k_3 - k)\delta^2$ follows. Let $g_e \in \mathcal{C}_3 \cap \mathcal{D}_3$ and $w \in \mathcal{G}(g_e, 3)$. Then $\delta + 2\varepsilon < \pi$ implies that $\rho_w(R_e)^2 = \rho_3(R_e)^2$, and hence

$$V_w(g_e) - V_3(g_e) \leq \frac{1}{2}(k - k_3)\rho_3(R_e)^2 + o.$$

Using $k - k_3 \leq 0$ and $\rho_3(R_e)^2 \geq \delta + \varepsilon > 0$, it holds that $o \leq \frac{1}{2}(k_3 - k)(\delta + \varepsilon)^2$.

(A8) For all $(g_e, q) \in \mathcal{C}$, it is clear that $\mathrm{d}V_q(g_e) = (R_e^\mathsf{T} K p_e, k_q \rho_q(R_e)) = 0$ if and only if $(g_e, q) \in \mathcal{A}$. ■

B. Potential functions on $\mathrm{SE}(3)$

Analogous to the surface vehicle case, we can identify the configuration of an underwater vehicle with the matrix Lie group $\mathrm{SE}(3) = \mathbb{R}^3 \rtimes \mathrm{SO}(3)$. An element $g = (p, R) \in \mathrm{SE}(3)$ contains the position $p \in \mathbb{R}^3$ and orientation $R \in \mathrm{SO}(3)$ of a vehicle-fixed frame with respect to an inertial frame.

The goal is to construct potential functions and a switching mechanism for stabilization of the configuration corresponding to the compact set

$$\mathcal{A}_0 = \{g_e \in \mathrm{SE}(3) : p_e = 0, R_e = I\}, \tag{53}$$

However, working with 3×3 rotation matrices can be cumbersome in practice. Unfortunately, there does not exist any globally nonsingular three-parameter representation of $\mathrm{SO}(3)$. As a result, practical state estimation and control applications normally utilize a globally nonsingular four-parameter unit quaternion representation of the vehicle orientation.

Unit quaternions $z = (\eta, \epsilon) \in \mathbb{S}^3$, where $\eta \in \mathbb{R}$ and $\epsilon \in \mathbb{R}^3$, map to the Lie group $\mathrm{SU}(2)$ through the isomorphism $z \mapsto Z$ defined by

$$Z \coloneqq \begin{pmatrix} \eta + i\epsilon_3 & -\epsilon_2 + i\epsilon_1 \\ \epsilon_2 + i\epsilon_1 & \eta - i\epsilon_3 \end{pmatrix} \in \mathbb{C}^{2\times 2}, \tag{54}$$

and an element $\omega = (\omega_1, \omega_2, \omega_3) \in \mathbb{R}^3$ maps to $\mathfrak{su}(2)$ through the isomorphism $(\cdot)^\wedge_{\mathfrak{su}(2)} \colon \mathbb{R}^3 \to \mathfrak{su}(2)$ defined by

$$\omega^\wedge_{\mathfrak{su}(2)} \coloneqq \frac{1}{2} \begin{pmatrix} i\omega_3 & -\omega_2 + i\omega_1 \\ \omega_2 + i\omega_1 & -i\omega_3 \end{pmatrix}. \tag{55}$$

The Lie algebras of $\mathfrak{su}(2)$ and $\mathfrak{so}(3)$ are isomorphic. Hence, the surjective homomorphism $\mathrm{Ad} \colon \mathrm{SU}(2) \to \mathrm{SO}(3)$ given by

$$\mathrm{Ad}_Z \coloneqq I_3 + 2\eta\epsilon^\wedge + 2(\epsilon^\wedge)^2, \tag{56}$$

is a covering map, where $(\cdot)^\wedge \colon \mathbb{R}^3 \to \mathfrak{so}(3)$ is defined by

$$\epsilon^\wedge \coloneqq \begin{pmatrix} 0 & -\epsilon_3 & \epsilon_2 \\ \epsilon_3 & 0 & -\epsilon_1 \\ -\epsilon_2 & \epsilon_1 & 0 \end{pmatrix}. \tag{57}$$

Note that $\mathrm{Ad} : \mathrm{SU}(2) \to \mathrm{SO}(3)$ is globally two-to-one and satisfies $\mathrm{Ad}_Z = \mathrm{Ad}_{-Z}$ because $\mathrm{SU}(2)$ is the double cover of $\mathrm{SO}(3)$. In practice, this implies that $\pm Z$ corresponds to the same physical orientation.

Using the adjoint action of $\mathrm{SU}(2)$ on $\mathbb{R}^3$ given by $(p, Z) \mapsto \mathrm{Ad}_Z\, p$, the semidirect product $\mathbb{R}^3 \rtimes \mathrm{SU}(2)$ implies that the natural error on $\widetilde{\mathrm{SE}}(3) \coloneqq \mathbb{R}^3 \rtimes \mathrm{SU}(2)$ is [28]

$$g_e = g_d^{-1} g = (p_e, Z_e) = (\mathrm{Ad}_{Z_d^{-1}}(p - p_d), Z_d^{-1} Z). \tag{58}$$

We remark that $\widetilde{\mathrm{SE}}(3)$ is the universal covering group of $\mathrm{SE}(3)$. Due to the double cover property of $\mathrm{SU}(2)$, stabilizing the set $\{g_e \in \widetilde{\mathrm{SE}}(3) : p_e = 0, Z_e = e\}$ using the gradient of a potential function either leads to unwinding, where the control law unnecessarily performs a full rotation of the rigid body, or it may lead to very poor convergence properties around $\mathrm{tr}(Z_e) = 2\eta_e = 0$ [10], [26], [36]. Consequently, to prevent unwinding and obtain global convergence properties, we must stabilize the compact set of disconnected points

$$\mathcal{A}^\circ = \{g_e \in \widetilde{\mathrm{SE}}(3) : Z_e = \pm e\}. \tag{59}$$

To this end, we define the set $Q \coloneqq \{-1, 1\}$ and the potential functions $V_q \colon \widetilde{\mathrm{SE}}(3) \to \mathbb{R}_{\geq 0}$ as in [26] by

$$\begin{aligned} V_q(g_e) &\coloneqq k\,\mathrm{tr}(e - qZ_e) + \tfrac{1}{2} p_e^\mathsf{T} K p_e \\ &= 2k(1 - q\eta_e) + \tfrac{1}{2} p_e^\mathsf{T} K p_e, \end{aligned} \tag{60}$$

where $k > 0$ and $K = K^\mathsf{T} > 0$. Let $\varepsilon \in (0, 1)$ denote the hysteresis half-width and define the flow and jump sets by

$$\mathcal{C} \coloneqq \{(g_e, q) \in \widetilde{\mathrm{SE}}(3) \times \mathcal{Q} : q\eta_e \geq -\varepsilon\} \tag{61a}$$

$$\mathcal{D} \coloneqq \{(g_e, q) \in \widetilde{\mathrm{SE}}(3) \times \mathcal{Q} : q\eta_e \leq -\varepsilon\}. \tag{61b}$$

Finally, the jump map is defined as

$$\mathcal{G}(q) \coloneqq -q. \tag{62}$$

Observe that the preceding definitions ensure that the switching is hysteretic since $q\eta_e \leq -\varepsilon$ implies that $\mathcal{G}(q)\eta_e \geq \varepsilon$.

Lemma 5: Let $\mathcal{A} \coloneqq \left\{(g_e, q) \in \widetilde{\mathrm{SE}}(3) \times \mathcal{Q} : \eta_e = q\right\}$. The 5-tuple $(\mathcal{A}, \mathcal{C}, \mathcal{D}, \mathcal{G}, V)$ satisfies Assumption 1.

Proof: The proof is a straightforward extension of the results of [26, Lemma 5.1, Theorem 5.2]. It is clear that the function $\check{V}_q : \mathbb{R}^3 \to \mathbb{R}$ defined by $p \mapsto \frac{1}{2} p^\mathsf{T} K p$ is continuously differentiable, radially unbounded and positive definite with respect to $\pi_{\mathbb{R}^3}(\mathcal{A})$. Moreover, $\mathcal{C}$ and $\mathcal{D}$ are clearly closed subsets of $\widetilde{\mathrm{SE}}(3) \times \mathcal{Q}$, $\mathcal{A}$ is compact, and for all $(g_e, q) \in \mathcal{C}$, it holds that $\mathrm{d}V_q(g_e) = (R_e^\mathsf{T} K p_e, kq\epsilon_e) = 0$ if and only if $p_e = 0, \epsilon_e = 0$ which implies that $\eta = \pm 1$, i.e., $(g_e, q) \in \mathcal{A}$. ■

VI. Experimental results

In this section we report the results of three experiments conducted in the Marine Cybernetics Laboratory (MC Lab) [37] at the Norwegian University of Science and Technology (NTNU) in Trondheim. The main purpose of the experiments is to demonstrate the applicability of the devised controllers in realistic scenarios for surface and submerged marine vehicles. The first two experiments were conducted using a scale model tug boat and the third experiment was conducted with a remotely operated underwater vehicle.

In the MC Lab, a local positioning system comprises sets of cameras mounted above and below the water surface and the Qualisys Track Manager (QTM) software. Light emitted by the cameras is reflected by a set of optical markers mounted on the vehicle to be tracked. These measurements are then processed with QTM, which outputs the position and orientation estimates at a rate of 100 Hz. A multiplicative extended Kalman filter (MEKF) [29, Section 14.4.3] is employed to reconstruct the velocities and filter the position and orientation. The MEKF is augmented with linear acceleration and angular velocity measurements for the underwater vehicle experiments.

Fig. 2. The Marine Cybernetics Lab at NTNU

Fig. 3. Cybership Enterprise in the MC-Lab

A. Cybership Enterprise

Cybership Enterprise (CSE) is a 1:50 scale model tug boat with a length of $1.105\,\mathrm{m}$ and beam of $0.248\,\mathrm{m}$. CSE is equipped with two Voith Schneider propellers (VSPs) and one bow thruster. The configuration of CSE is described by $g = (p, R) \in \mathrm{SE}(2)$, where elements in $\mathrm{SE}(2)$ admit a homogeneous matrix representation through the injective homomorphism $\mathrm{SE}(2) \to \mathrm{GL}(3)$ defined by [28]

$$g \coloneqq \begin{pmatrix} R & p \\ 0 & 1 \end{pmatrix} \in \mathbb{R}^{3\times 3}. \tag{63}$$

Denoting the vehicle-fixed linear and angular velocities by $v \in \mathbb{R}^2$ and $\omega \in \mathbb{R}$, respectively, define the vehicle-fixed velocity as $\nu \coloneqq (v, \omega) \in \mathbb{R}^3$. An element $\nu \in \mathbb{R}^3$ maps to $\mathfrak{se}(2)$ through the isomorphism $(\cdot)^\wedge \colon \mathbb{R}^3 \to \mathfrak{se}(2)$ defined by

$$\nu^\wedge \coloneqq \begin{pmatrix} S\omega & v \\ 0 & 0 \end{pmatrix} \in \mathbb{R}^{3\times 3}, \quad S \coloneqq \begin{pmatrix} 0 & -1 \\ 1 & 0 \end{pmatrix}. \tag{64}$$

Let $\theta \in \mathbb{R}^{15}$ denote the model parameters. The equations of motion for a surface vehicle can be formulated by (2) with

$$M = \begin{pmatrix} \theta_1 & 0 & 0 \\ 0 & \theta_2 & \theta_3 \\ 0 & \theta_3 & \theta_4 \end{pmatrix}, \quad f(g) = b, \tag{65}$$

$$d(\nu) = \begin{pmatrix} -\theta_5\nu_1 \\ -\theta_6\nu_2 - \theta_8\omega \\ -\theta_9\nu_2 - \theta_7\omega \end{pmatrix} + \begin{pmatrix} -\theta_{10}|\nu_1|\nu_1 \\ -\theta_{11}|\nu_2|\nu_2 \\ -\theta_{12}|\omega|\omega \end{pmatrix} \tag{66}$$

where $b = (\theta_{13}, \theta_{14}, \theta_{15}) \in \mathbb{R}^3$ is a constant bias. We remark that the expression for the regressor Φ follows from (18) together with (65) and (66).

The generalized forces are calculated using (27), where the adjoint actions of $\mathrm{SE}(2)$ and $\mathfrak{se}(2)$ on $\mathbb{R}^3$ for $g = (p, R) \in \mathrm{SE}(2)$ and $\nu = (v, \omega) \in \mathbb{R}^3$ are given by

$$\mathrm{Ad}_g = \begin{pmatrix} R & -Sp \\ 0 & 1 \end{pmatrix}, \quad \mathrm{ad}_\nu = \begin{pmatrix} S\omega & -Sv \\ 0 & 0 \end{pmatrix}. \tag{67}$$

TABLE I
CONTROL PARAMETERS

Circle		Lemniscate	
δ	$\pi/6$	δ	$\pi/18$
ε	$\pi/18$	ε	$\pi/18$
K_p	$\mathrm{diag}(1.7, 1.7)$	K_p	$\mathrm{diag}(1.45, 1.45)$
k	0.5	k	0.5
k_3	1.2	k_3	1.5
K_d	$\mathrm{diag}(.7, .6, .6)$	K_d	$\mathrm{diag}(1.25, 1.25, 1)$
Λ	I_3	Λ	I_3

The generalized forces $\tau \in \mathbb{R}^3$ map to the actuator inputs $(\alpha, u) \in \mathbb{R}^2 \times \mathbb{R}^3$ through

$$\tau = B(\alpha)Ku, \tag{68}$$

where $\alpha = (\alpha_1, \alpha_2)$ are the VSP angles and $u = (u_1, u_2, u_3)$ are the thruster inputs. Specifically, (u_1, u_2) corresponds to the VSPs, and u_3 is the bow thruster.

Using the transformation $(\alpha, u) \mapsto (\check{u}_1, \check{u}_2, \check{u}_3)$, where

$$\check{u}_1 = \begin{pmatrix} \cos(\alpha_1)u_1 \\ \sin(\alpha_1)u_1 \end{pmatrix}, \check{u}_2 = \begin{pmatrix} \cos(\alpha_2)u_2 \\ \sin(\alpha_2)u_2 \end{pmatrix}, \check{u}_3 = u_3. \tag{69}$$

we can rewrite (68) as $\tau = \check{B}\check{K}\check{u}$, which is solved using the Moore-Penrose pseudoinverse

$$\check{u}_* = (\check{B}\check{K})^\dagger \tau, \tag{70}$$

for a given $\tau \in \mathbb{R}^3$. The actuator control inputs (α, u) are then obtained by inverting the transformation (69). Note that the BT input is constrained to the interval $[-1, 1]$, while the VSP inputs are constrained to $[0, 1]$. The desired path is given by $\gamma(s) = (\gamma_1(s), \gamma_2(s)) \in \mathrm{SE}(2)$ where

$$\gamma_1(s) = \begin{pmatrix} x_d(s) \\ y_d(s) \end{pmatrix}, \gamma_2(s) = \exp(S\psi_d(s)), \tag{71}$$

where $\psi_d(s) = \mathrm{atan2}(y_d'(s), x_d'(s))$.

The hysteresis width and control gains are chosen according to Table I with $\vartheta_q(\zeta) = K_d\zeta$ and $\varphi_q(\xi) = K_d\xi$. Moreover, the adaptation gain and bounds on $\theta \in \mathbb{R}^{15}$ are given by

$$\begin{aligned} \Gamma &= \mathrm{blkdiag}(50, 40, 5, 20, 5I_{4\times 4}, 10I_{9\times 9}, 0.025, 0.1, 0.01), \\ \underline{\theta} &= (10, 15, 1, -3, 0_{7\times 1}, -1, -4, -4, -4), \\ \overline{\theta} &= (20, 30, 5, 3, 10_{7\times 1}, 10, 4, 4, 4), \end{aligned}$$

and the parameters are initialized as

$$\theta_0 = (10, 15, 1, 0_{12\times 1}). \tag{72}$$

Two two experiments are performed using different parametrized loops; the first loop is a circle, and the second is a lemniscate.

1) Circle: The circle is centered at $O = (1\,\mathrm{m}, 0)$ with a radius of $R = 1.2\,\mathrm{m}$ and is represented by the parametric equation

$$\gamma_1(s) = \begin{pmatrix} R\cos(s) \\ R\sin(s) \end{pmatrix} + O. \tag{73}$$

Experimental results are presented in Figures 4 to 10. The ship was initialized at $p(0) = (0.35\,\mathrm{m}, -1.46\,\mathrm{m})$ with $\psi = -42°$. At this point in time, the orientation error was $\rho_3(R_e(t))|_{t=0} = -\pi\frac{106}{180} \geq \delta + \varepsilon$, and it follows from (47)

This article has been accepted for publication in IEEE Transactions on Automatic Control. This is the author's version which has not been fully edited and content may change prior to final publication. Citation information: DOI 10.1109/TAC.2022.3161372

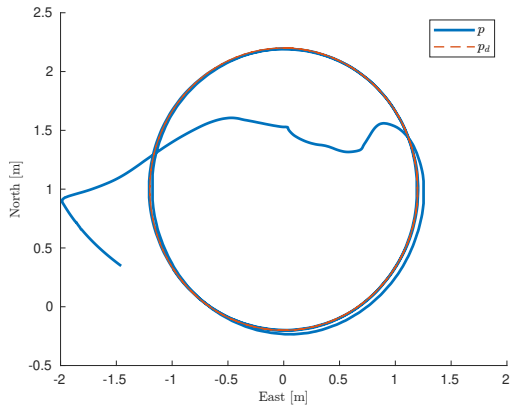

Fig. 4. North-East plot showing the North-East position $\boldsymbol{p} = (\boldsymbol{x}, \boldsymbol{y})$ and the desired position $\boldsymbol{p_d} = (\boldsymbol{x_d}, \boldsymbol{y_d})$.

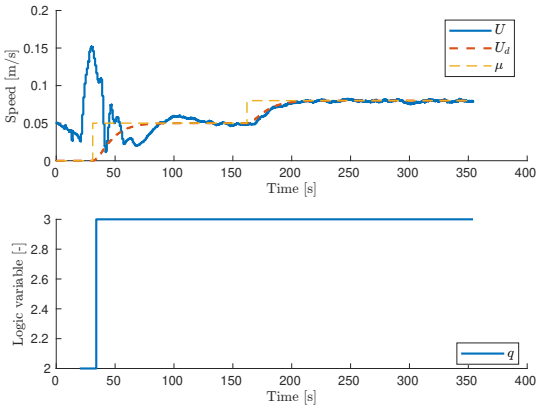

Fig. 7. The speed $\boldsymbol{U}$, desired speed $\boldsymbol{u_d}$, commanded input speed $\boldsymbol{\mu}$ and logic variable $\boldsymbol{q}$.

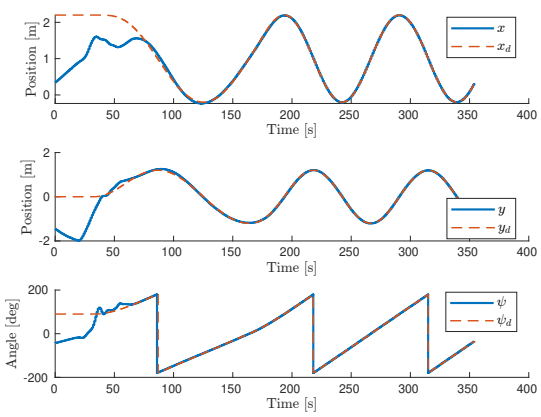

Fig. 5. The configuration $\boldsymbol{p} = (\boldsymbol{x}, \boldsymbol{y}), \boldsymbol{R} = \mathbf{exp}(\boldsymbol{S\psi})$ and the desired configuration $\boldsymbol{p_d} = (\boldsymbol{x_d}, \boldsymbol{y_d}), \boldsymbol{R_d} = \mathbf{exp}(\boldsymbol{S\psi_d})$.

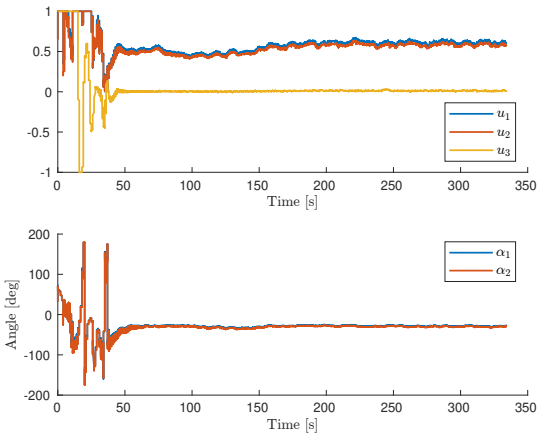

Fig. 8. The VSP control inputs $\boldsymbol{u_1}, \boldsymbol{u_2} \in [\mathbf{0}, \mathbf{1}]$, the BT control input $\boldsymbol{u_3} \in [-\mathbf{1}, \mathbf{1}]$ and VSP angle inputs $\boldsymbol{\alpha_1}, \boldsymbol{\alpha_2}$.

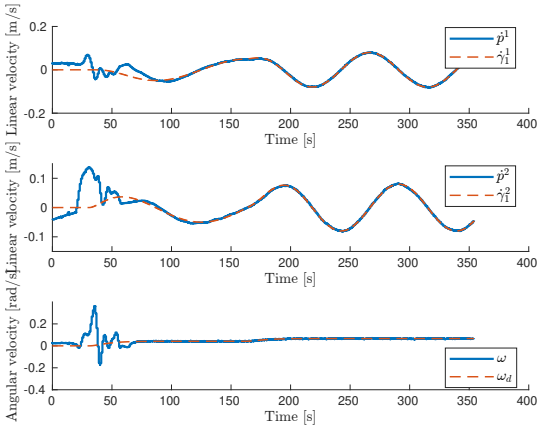

Fig. 6. The velocity estimates $(\dot{\boldsymbol{p}}, \boldsymbol{\omega})$ and the desired velocity references $(\dot{\boldsymbol{\gamma}}_\mathbf{1}, \boldsymbol{\omega_d})$.

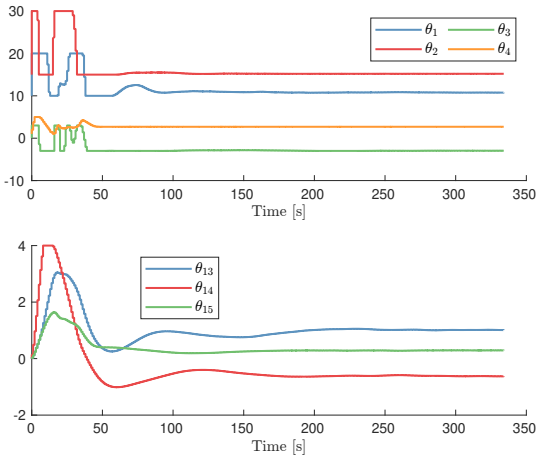

Fig. 9. The inertia and bias parameters.

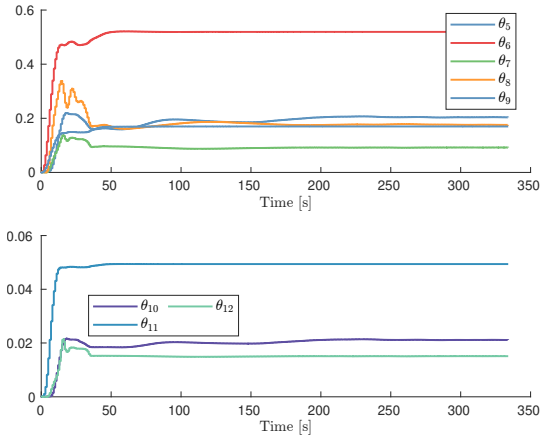

Fig. 10. The damping parameters associated with the linear and nonlinear damping.

that $\rho_2^2(R_e(t))|_{t=0} < \rho_1^2(R_e(t))|_{t=0}$. In other words, the orientation error was in the jump set corresponding to $q = 3$ and the jump map (51) implies that the global controller corresponding to $q^+ = 2$ was activated, which is what we observe in the lower plot in Figure 7. Then, at $t \approx 33\,\mathrm{s}$, the commanded input speed μ was set to $0.08\,\mathrm{m/s}$ as seen in Figure 7. Figures 4 and 5 shows that CSE accurately tracked the path after an initial transient due to the significant initial configuration error, even though the actuator inputs saturate until $t \approx 25\,\mathrm{s}$ as seen in Figure 8. Figure 6 depicts the system velocities and desired velocities, while Figure 7 shows the commanded input speed $\mu(t)$, the desired speed $u_d(t)$ and the estimated speed $U(t) = \|v(t)\|$. Therefore, it is clear that the speed and velocities are tracked with sufficient accuracy.

2) Lemniscate: The lemniscate is centered at $O = (2\,\mathrm{m}, 0)$ and is represented by the parametric equation

$$\gamma_1(s) = \begin{pmatrix} R_1 \dfrac{\cos s}{1+\sin^2 s} \\ R_2 \dfrac{\sqrt{2}\sin 2s}{1+\sin^2 s} \end{pmatrix} + O, \tag{74}$$

where $R_1 = 2\,\mathrm{m}$, $R_2 = 2.4\,\mathrm{m}$.

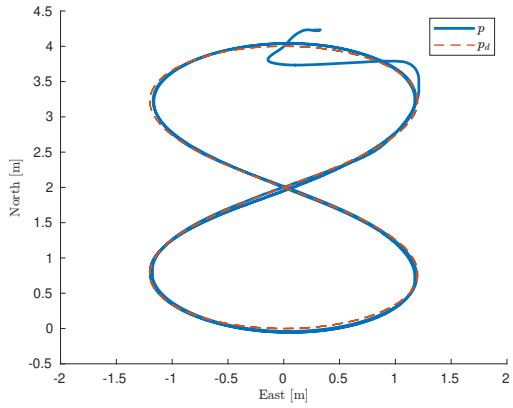

Fig. 11. North-East plot showing the position $\boldsymbol{p}$ and the desired position $\boldsymbol{p_d}$.

Experimental results are presented in Figures 11 to 17. The ship was initialized at $p(0) = (4.2\,\mathrm{m}, 0.3\,\mathrm{m})$ with a heading

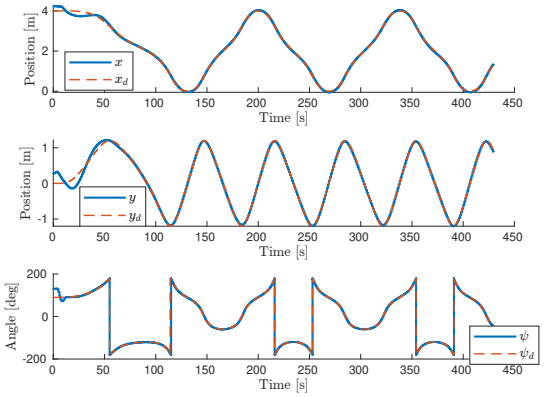

Fig. 12. The configuration $\boldsymbol{p} = (\boldsymbol{x}, \boldsymbol{y})$, $\boldsymbol{R} = \exp(\boldsymbol{S\psi})$ and the desired configuration $\boldsymbol{p_d} = (\boldsymbol{x_d}, \boldsymbol{y_d})$, $\boldsymbol{R_d} = \exp(\boldsymbol{S\psi_d})$.

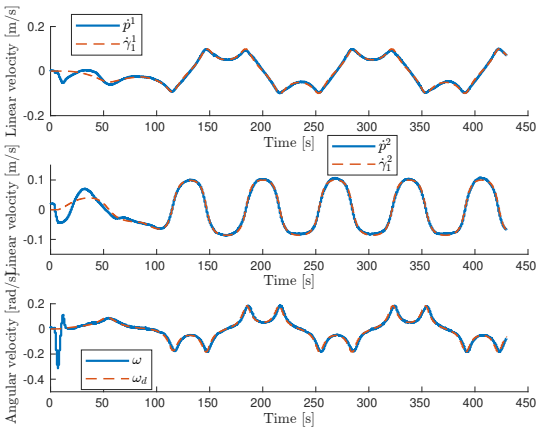

Fig. 13. The velocity estimates $(\dot{\boldsymbol{p}}, \boldsymbol{\omega})$ and the desired velocity references $(\dot{\boldsymbol{\gamma}}_1, \boldsymbol{\omega_d})$.

of $\psi = 130°$. Since the lemniscate loop given by (74) does not result in a constant acceleration with respect to the body-fixed frame for nonzero commanded input speeds, the control gains must be increased to compensate for the inaccuracies in the dynamic model and obtain similar performance to the circular trajectory.

By comparing Figures 9 and 10 with Figures 16 and 17, it is clear that the parameters do not converge to any 'true' value. This cannot be expected because we have not provided any persistency of excitation condition; that is, we have not given any conditions under which (27) uniformly globally asymptotically stabilizes the compact set $\widetilde{\mathcal{B}}$ for the closed-loop system $\mathscr{H}$. However, even if such conditions were provided, a constant bias in the vehicle-fixed frame will not fully capture the inaccuracies in the mapping between the forces produced by the actuators and their inputs. As a consequence, the desired forces and torque computed by the control law are significantly different from the actual forces and torque produced by the actuators. In turn, this leads to a tracking error, which induces parameter adaptation. Since this adaptation occurs due to unmodeled effects that are not correctly captured by our assumed model structure, we cannot expect to accurately identify the mass and damping model parameters for this system. Instead, due to the presence of a constant bias in our dynamic model, our control law is more reminiscent of a PID

This article has been accepted for publication in IEEE Transactions on Automatic Control. This is the author's version which has not been fully edited and content may change prior to final publication. Citation information: DOI 10.1109/TAC.2022.3161372

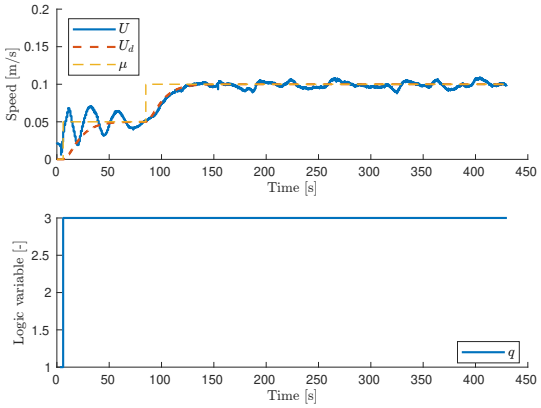

Fig. 14. The speed $\boldsymbol{U}$, desired speed $\boldsymbol{u_d}$, commanded input speed $\boldsymbol{\mu}$ and logic variable $\boldsymbol{q}$.

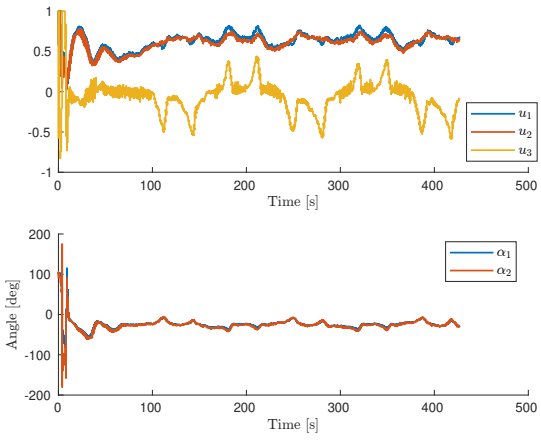

Fig. 15. The VSP control inputs $\boldsymbol{u_1, u_2} \in [\mathbf{0}, \mathbf{1}]$, the BT control input $\boldsymbol{u_3} \in [-\mathbf{1}, \mathbf{1}]$ and VSP angle inputs $\boldsymbol{\alpha_1, \alpha_2}$.

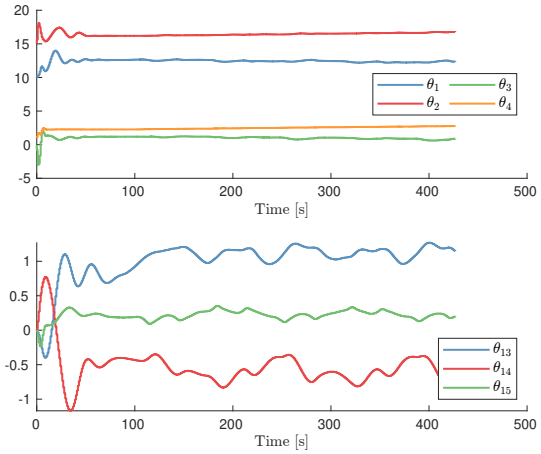

Fig. 16. The inertia and bias parameters.

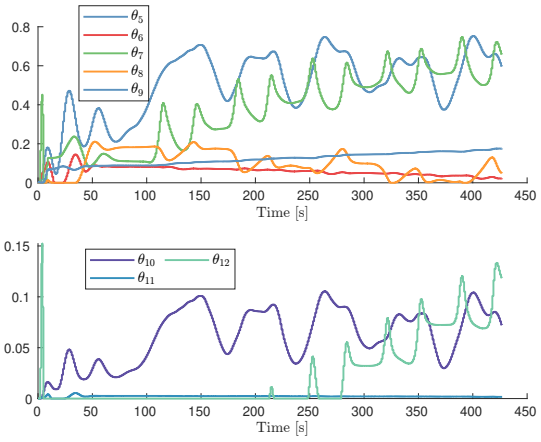

Fig. 17. The damping parameters associated with the linear and nonlinear damping.

controller with adaptive feedforward. To see this, note that the bias feedforward term can be written as $-\int_0^t(\nu_e(\tau)-\zeta(\tau))\mathrm{d}\tau$, and that (15) can be interpreted as a multiple-input multiple-output low-pass filter with input $-\mathrm{d}V_q$ and output ζ. Thus, when the velocity error ν_e is zero, the bias feedforward term can be interpreted as the integral of the output of a low-pass filter whose input is the configuration error.

Finally, we observe that the parameters converge for the circular trajectory. This is a consequence of the steady-state nature of the circular trajectory, that is, constant desired velocities with respect to the desired frame when u_d has converged to the commanded input speed μ. For the lemniscate trajectory, however, the desired velocities are not constant even if the desired speed has converged to the commanded input speed. Hence, considering the inaccuracies in the mappings between the desired forces and torque and the produced forces and torque, it is not surprising that the parameters do not converge to any specific values and that the damping and bias parameters change more rapidly when the ship is in a turning maneuver, as seen in Figures 12, 16 and 17. Despite these structural modeling inaccuracies, the ship's position remains within $4\,\mathrm{cm}$ of the desired position after converging to the path, as seen in Figures 11 and 12. Moreover, from Figure 13 and Figure 14, we observe that the desired velocities and the desired speed are tracked with sufficient accuracies.

B. BlueROV2

The BlueROV2 is a remotely operated underwater vehicle developed by Blue Robotics. The experiments were conducted using the heavy configuration BlueROV2 with eight thrusters, depicted in Fig. 18.

Elements $g = (p, Z) \in \widetilde{\mathrm{SE}}(3)$ admit a matrix representation using the injective homomorphism $\widetilde{\mathrm{SE}}(3) \to \mathrm{GL}(6, \mathbb{C})$ given by

$$g = \begin{pmatrix} \mathrm{Ad}_Z & p & 0 \\ 0 & 1 & 0 \\ 0 & 0 & Z \end{pmatrix} \in \mathbb{C}^{6\times 6} \tag{75}$$

Denoting the vehicle-fixed linear and angular velocities by $v \in \mathbb{R}^3$ and $\omega \in \mathbb{R}^3$, respectively, define the vehicle-fixed velocity

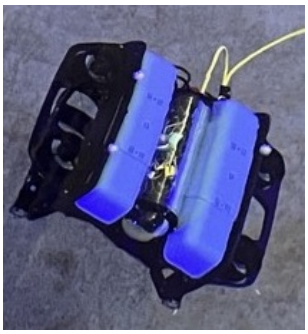

Fig. 18. The BlueROV2 in the MC-Lab.

as $\nu := (v, \omega) \in \mathbb{R}^6$. An element $\nu \in \mathbb{R}^6$ maps to $\widetilde{\mathfrak{se}}(3)$ through the isomorphism $(\cdot)^\wedge \colon \mathbb{R}^6 \to \widetilde{\mathfrak{se}}(3)$ defined by

$$\nu^\wedge = \begin{pmatrix} \omega^\wedge & v & 0 \\ 0 & 0 & 0 \\ 0 & 0 & \omega^\wedge_{\mathfrak{su}} \end{pmatrix} \in \mathbb{C}^{6\times 6}. \tag{76}$$

The equations of motion for an underwater vehicle can then be formulated by (2) with

$$f(g) = \beta(Z) + b, \tag{77}$$

where $\beta(Z) = (\theta_7 \operatorname{Ad}_Z^\mathsf{T} e_3, e_3^\wedge \operatorname{Ad}_Z^\mathsf{T} \theta_{8:10})$ contains gravitational and buoyancy forces and $b = (\theta_1, \dots, \theta_6) \in \mathbb{R}^6$ is a constant bias. Moreover, by assuming port/starboard and fore/aft symmetry, the inertia matrix is parametrized by

$$M = \begin{pmatrix} \theta_{11} & 0 & 0 & 0 & \theta_{17} & 0 \\ 0 & \theta_{12} & 0 & \theta_{18} & 0 & 0 \\ 0 & 0 & \theta_{13} & 0 & 0 & 0 \\ 0 & \theta_{18} & 0 & \theta_{14} & 0 & 0 \\ \theta_{17} & 0 & 0 & 0 & \theta_{15} & 0 \\ 0 & 0 & 0 & 0 & 0 & \theta_{16} \end{pmatrix} \tag{78}$$

while the hydrodynamic drag forces are assumed to satisfy

$$d_i(\nu) = \theta_{18+i} + \theta_{24+i}|\nu_i|\nu_i, \tag{79}$$

for $i \in \{1, \dots, 6\}$. We remark that the expression for the regressor Φ follows from (18) together with (77), (78) and (79). The generalized forces are calculated using the control law (27), where the adjoint actions of $\widetilde{\mathrm{SE}}(3)$ and $\widetilde{\mathfrak{se}}(3)$ on $\mathbb{R}^6$ for $g = (p, Z) \in \widetilde{\mathrm{SE}}(3)$ and $\nu = (v, \omega) \in \mathbb{R}^6$ are given by

$$\operatorname{Ad}_g = \begin{pmatrix} \operatorname{Ad}_Z & p^\wedge \operatorname{Ad}_Z \\ 0 & \operatorname{Ad}_Z \end{pmatrix}, \quad \operatorname{ad}_\nu = \begin{pmatrix} \omega^\wedge & v^\wedge \\ 0 & \omega^\wedge \end{pmatrix}. \tag{80}$$

The generalized forces $\tau \in \mathbb{R}^6$ map to the desired thrust $u \in \mathbb{R}^8$ through $\tau = Ku$, where each column of K is

$$K_i = \begin{pmatrix} r_i \\ L_i \times r_i \end{pmatrix}, \tag{81}$$

where $r_i \in \mathbb{R}^3$ is a unit vector pointing in the direction of thrust and $L_i \in \mathbb{R}^3$ is the position of the thruster relative to the body frame. Using (27), the actuator control inputs are then found from the expression $u = K^\dagger \tau$.

The desired path is given by $\gamma(s) = (p_d(s), Z_d(s)) \in \widetilde{\mathrm{SE}}(3)$, with

$$p_d(s) = \begin{pmatrix} L_1 \frac{\cos s}{1+\sin^2 s} \\ L_2 \frac{\sqrt{2}\sin 2s}{1+\sin^2 s} \\ L_3 \frac{2\sin s}{1+\sin^2 s} \end{pmatrix} + O,\ z_d(s) = \begin{pmatrix} \cos(\psi(s)/2) \\ 0 \\ 0 \\ \sin(\psi(s)/2) \end{pmatrix}$$

where z_d is a unit quaternion that maps to $\mathrm{SU}(2)$ through the isomorphism $z_d \mapsto Z_d$ defined in (54). Moreover, $L_1 = 1\,\mathrm{m}$, $L_2 = 0.6\,\mathrm{m}$, $L_3 = 0.25\,\mathrm{m}$, $O = (0.2\,\mathrm{m}, -0.3\,\mathrm{m}, -0.55\,\mathrm{m})$ and $\psi(s) = \operatorname{atan2}(y_d'(s), x_d'(s))$.

The desired speed reference is given by

$$\mu = \begin{cases} 0.1\,\mathrm{m/s}, & 5 \le t < 125 \\ 0.2\,\mathrm{m/s}, & t \ge 125 \end{cases}, \tag{82}$$

while the hysteresis half-width is $\varepsilon = 0.1$. The control gains are chosen as $K_p = \operatorname{diag}(50, 50, 70), k = 16, \varphi_q(\xi) = K_d\xi, \vartheta_q(\zeta) = K_d\zeta$ and $\Lambda = I_6$ with $K_d = \operatorname{diag}(40, 40, 30, 7, 7, 7)$. Moreover, the adaptation gain and bounds on $\theta \in \mathbb{R}^{30}$ are given by

$$\begin{aligned} \Gamma &= \operatorname{blkdiag}(\Gamma_1, \Gamma_2, \Gamma_3), \\ \Gamma_1 &= \operatorname{diag}(1.5, 1.5, 1.5, 1.2, 1.2, 1.2), \\ \Gamma_2 &= \operatorname{diag}(2.5, 2, 2, 2), \\ \Gamma_3 &= \operatorname{diag}(7, 7, 7, 4, 4, 4, 5, 5, 20, 20, 20, 5, 5, 5, \\ &\qquad 20, 20, 20, 5, 5, 5), \\ \underline{\theta} &= (-40, -10_{9\times 1}, 0_{7\times 1}, -2, 0_{12\times 1}), \\ \overline{\theta} &= (10_{10\times 1}, 50_{6\times 1}, 2, 0, 50_{12\times 1}), \end{aligned}$$

and the parameters are initialized as

$$\begin{aligned} \theta_0 = (&0_{10\times 1}, 19.17, 26.37, 28.24, 0.28, 0.28, \\ &0.28, 0.23, -0.23, 4.03, 6.22, 5.1, \\ &0.07, 0.07, 0.07, 18.18, 21.66, 36.99, \\ &1.55, 1.55, 1.55) \end{aligned} \tag{83}$$

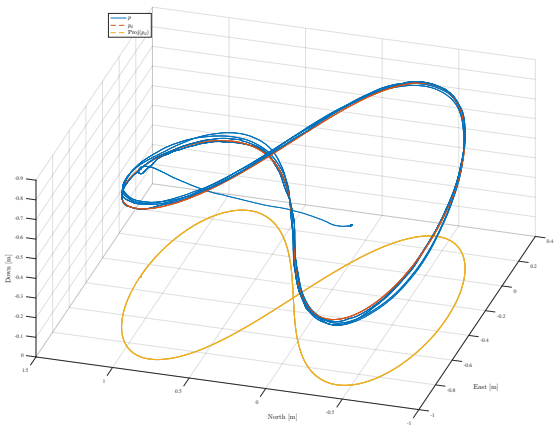

Fig. 19. North-East-Down plot showing the position $\boldsymbol{p}$, the desired position $\boldsymbol{p_d}$ and the projection of $\boldsymbol{p_d}$ onto the North-East plane.

Experimental results are presented in Figures 19 to 27. Due to limitations in the hardware implementation, the controller activates a few seconds before the data logger and actuator

This article has been accepted for publication in IEEE Transactions on Automatic Control. This is the author's version which has not been fully edited and content may change prior to final publication. Citation information: DOI 10.1109/TAC.2022.3161372

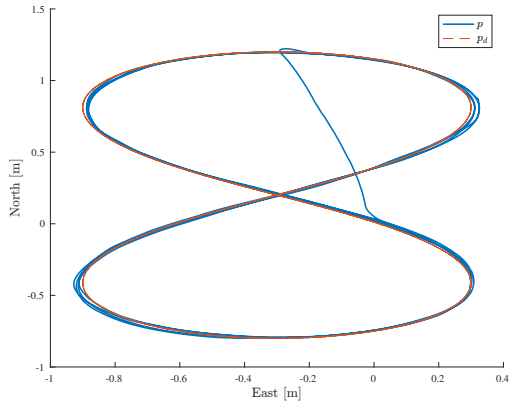

Fig. 20. North-East plot of the position and desired position

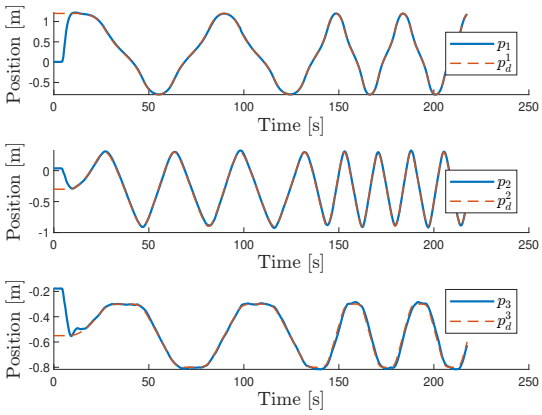

Fig. 21. The position $\boldsymbol{p} = (\boldsymbol{p_1}, \boldsymbol{p_2}, \boldsymbol{p_3})$ and desired position $\boldsymbol{p_d} = (\boldsymbol{p_d^1}, \boldsymbol{p_d^2}, \boldsymbol{p_d^3})$.

driver do. As a result, the bias and gravitational parameters have already adapted for several seconds by the time the control signals are sent to the actuators. This can be observed in the upper plot in Figure 27, where θ_1 and θ_3, i.e., the x and z components of the bias, are already saturated at $t \approx 4\,\mathrm{s}$ when the actuator driver is activated and the control inputs are converted to pulse width modulated actuator signals. Remarkably, this has little effect on the transient performance, as observed in Figure 21. This occurs despite the fact that the BlueROV2 was initialized at the bottom of the pool at a distance $\|p_e\| \approx 1.36\,\mathrm{m}$ away from the desired position with no initial knowledge of the gravitational- and buoyancy-related parameters.

The initial quaternion error satisfies $\eta_e \leq -\varepsilon$, which entails that a switch from the initial value of $q = 1$ to $q = -1$ occurs at the first time step of the controller. Since the logger was initialized after the controller, although no control inputs were sent to the actuators, we have changed first logged value of the logic variable to $q = 1$ to highlight the fact that a switch has in fact occurred.

From Figures 19, 21 and 22, we observe that the ROV successfully tracks the position and orientation references with satisfactory accuracy. Moreover, from Figures 23 and 24, we see that the desired velocities $\nu_r = \mathrm{Ad}_{g_e^{-1}}\,\nu_d$ are tracked with satisfactory accuracy. However, we remark that v_3 contains significantly more noise compared to the other linear veloc-

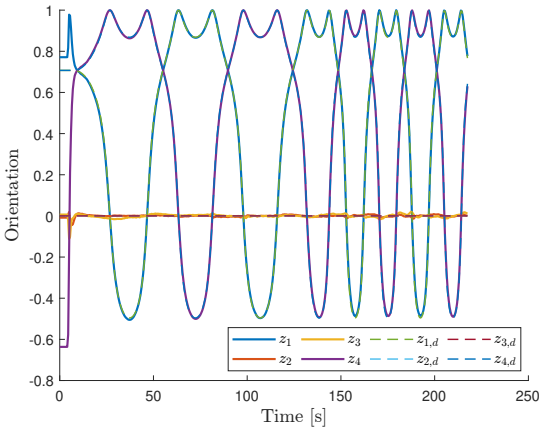

Fig. 22. The orientation and desired orientation, represented by the unit quaternions $\boldsymbol{z}$ and $\boldsymbol{z_d}$, respectively.

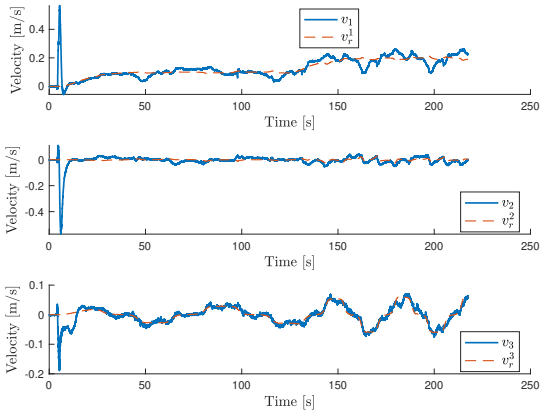

Fig. 23. The linear velocities $\boldsymbol{v}$ and the desired linear velocities $\boldsymbol{v_r}$, decomposed in the body frame.

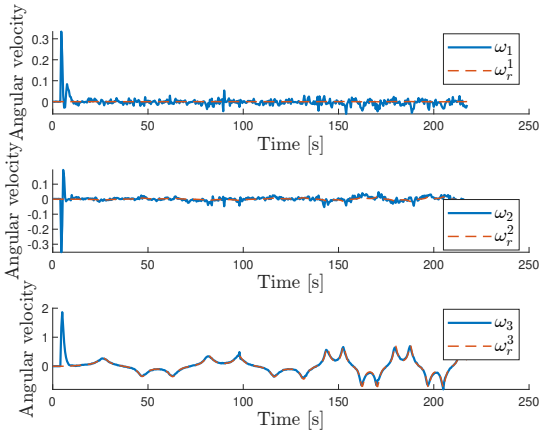

Fig. 24. The angular velocities $\boldsymbol{\omega}$ and the desired angular velocities $\boldsymbol{\omega_r}$ decomposed in the body frame.

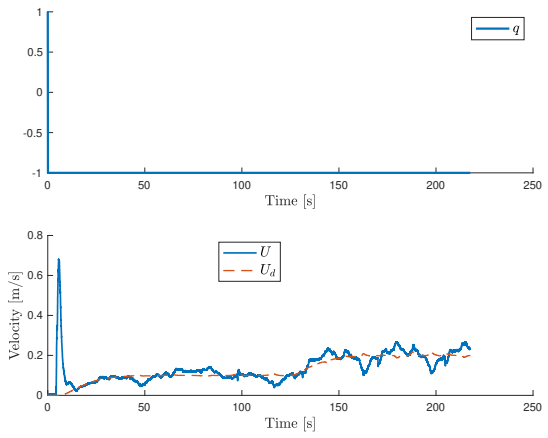

Fig. 25. The logic variable $\boldsymbol{q}$, the speed $\boldsymbol{U}$, and the desired speed $\boldsymbol{U_d = |\dot{\gamma}_1|}$

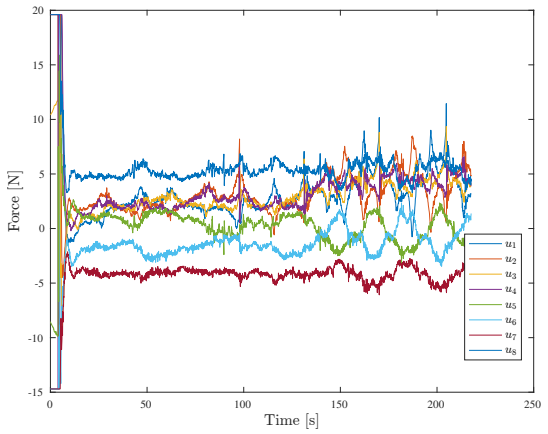

Fig. 26. The control inputs $\boldsymbol{u}$ corresponding to the eight thrusters.

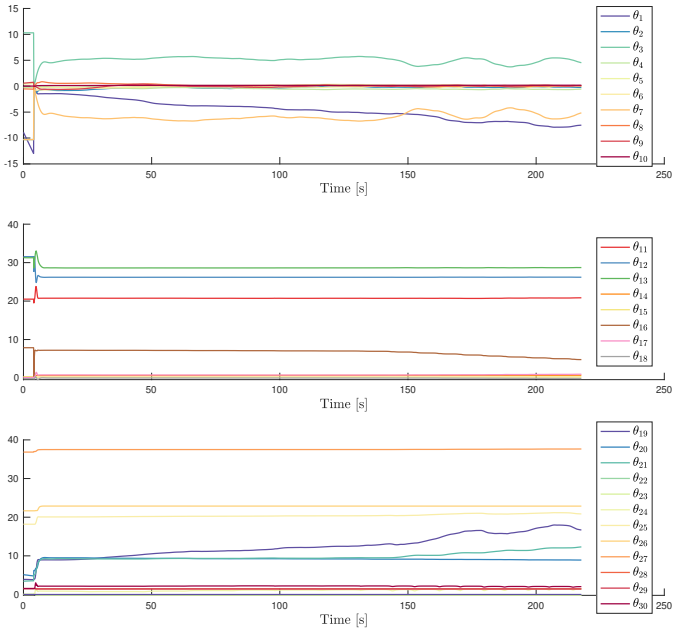

Fig. 27. The bias and gravitational/buoyancy related parameters, the inertia matrix parameters and the damping parameters.

ities. Moreover, the x-component of the linear velocity, v_1, exhibits spikes that coincide with the minima of p_3, i.e. the z-component of the position vector. This is due to poor tracking of the ROV from the camera-based underwater positioning system, which either loses track of the ROV and/or outputs noisy and inaccurate position measurements (especially in the z-direction). This can be mitigated by further restricting the operating region of the ROV and/or lowering the weight of the camera-based position measurements relative to the accelerometer measurements in the Kalman filter.

VII. Conclusion

In this paper, we have proposed an adaptive hybrid feedback control law for marine vehicles. The control law tracks a hybrid reference system constructed from a parametrized loop and a speed assignment for the motion along the path and achieves global asymptotic tracking of the loop at a time-varying desired speed. The proposed hybrid feedback control law was implemented on a scale model tug boat and a remotely operated underwater vehicle, and laboratory experiments have demonstrated the effectiveness of the proposed control law.

References

[1] S. P. Bhat and D. S. Bernstein, "A topological obstruction to continuous global stabilization of rotational motion and the unwinding phenomenon," *Systems & Control Letters*, vol. 39, no. 1, pp. 63 – 70, 2000.

[2] A. R. Teel, "Robust hybrid control systems: An overview of some recent results," in *Advances in Control Theory and Applications*, C. Bonivento, A. Isidori, L. Marconi, and C. Rossi, Eds. Springer, 2007, pp. 279–302.

[3] C. G. Mayhew and A. R. Teel, "Hybrid control of rigid-body attitude with synergistic potential functions," in *Proc. 2011 American Control Conf.*, San Francisco, CA, USA, 2011.

[4] C. G. Mayhew, R. G. Sanfelice, and A. R. Teel, "Synergistic Lyapunov functions and backstepping hybrid feedbacks," in *Proc. 2011 American Control Conf.*, San Francisco, CA, USA, June 2011.

[5] C. G. Mayhew and A. R. Teel, "Hybrid control of planar rotations," in *Proc. 2010 American Control Conf.*, Baltimore, MD, USA, 2010.

[6] M. Marley, R. Skjetne, and A. R. Teel, "A kinematic hybrid feedback controller on the unit circle suitable for orientation control of ships," in *Proc. 59th Conf. on Decision and Control*, Jeju Island, Republic of Korea, 2020.

[7] C. G. Mayhew and A. R. Teel, "Hybrid control of spherical orientation," in *Proc. 49th IEEE Conference on Decision and Control*, Atlanta, GA, USA, 2010.

[8] ——, "Synergistic hybrid feedback for global rigid-body attitude tracking on SO(3)," *IEEE Transactions on Automatic Control*, vol. 58, no. 11, pp. 2730–2742, Nov 2013.

[9] S. Berkane and A. Tayebi, "Construction of synergistic potential functions on SO(3) with application to velocity-free hybrid attitude stabilization," *IEEE Transactions on Automatic Control*, vol. 62, no. 1, pp. 495–501, 2017.

[10] E. A. Basso, H. M. Schmidt-Didlaukies, and K. Y. Pettersen, "Hysteretic control Lyapunov functions with application to global asymptotic tracking for underwater vehicles," in *Proc. 59th Conf. on Decision and Control*, Jeju Island, Republic of Korea, 2020.

[11] P. Casau, R. Cunha, R. G. Sanfelice, and C. Silvestre, "Hybrid control for robust and global tracking on smooth manifolds," *IEEE Transactions on Automatic Control*, vol. 65, no. 5, pp. 1870–1885, 2020.

[12] T. Lee, "Global exponential attitude tracking controls on SO(3)," *IEEE Transactions on Automatic Control*, vol. 60, no. 10, 2015.

[13] P. Casau, R. G. Sanfelice, and C. Silvestre, "Adaptive backstepping of synergistic hybrid feedbacks with application to obstacle avoidance," in *Proc. 2019 American Control Conf.*, Philadelphia, PA, USA, 2019.

[14] T. I. Fossen and S. I. Sagatun, "Adaptive control of nonlinear underwater robotic systems," in *Proc. 1991 IEEE International Conference on Robotics and Automation*, Sacramento, CA, USA, 1991.

[15] T. I. Fossen and O.-E. Fjellstad, "Robust adaptive control of underwater vehicles: A comparative study," in *Proc. 3rd IFAC Workshop on Control Applications in Marine Systems*, Trondheim, Norway, 1995.
[16] O.-E. Fjellstad and T. Fossen, "Position and attitude tracking of AUV's: a quaternion feedback approach," *IEEE Journal of Oceanic Engineering*, vol. 19, no. 4, pp. 512–518, 1994.
[17] G. Antonelli, F. Caccavale, S. Chiaverini, and G. Fusco, "A novel adaptive control law for underwater vehicles," *IEEE Transactions on control systems technology*, vol. 11, no. 2, pp. 221–232, 2003.
[18] G. Antonelli, S. Chiaverini, N. Sarkar, and M. West, "Adaptive control of an autonomous underwater vehicle: experimental results on ODIN," *IEEE Transactions on Control Systems Technology*, vol. 9, no. 5, pp. 756–765, 2001.
[19] J.-M. Godhavn, T. I. Fossen, and S. P. Berge, "Non-linear and adaptive backstepping designs for tracking control of ships," *International Journal of Adaptive Control and Signal Processing*, 1998.
[20] R. Skjetne, O. Smogeli, and T. Fossen, "A nonlinear ship manoeuvering model: Identification and adaptive control with experiments for a model ship," *Modeling, Identification and Control*, vol. 25, pp. 3–27, 2004.
[21] R. Skjetne, T. I. Fossen, and P. V. Kokotović, "Adaptive maneuvering, with experiments, for a model ship in a marine control laboratory," *Automatica*, vol. 41, no. 2, pp. 289–298, 2005.
[22] A. H. Brodtkorb, S. A. Værnø, A. R. Teel, A. J. Sørensen, and R. Skjetne, "Hybrid controller concept for dynamic positioning of marine vessels with experimental results," *Automatica*, 2018.
[23] R. Skjetne, T. I. Fossen, and P. V. Kokotović, "Robust output maneuvering for a class of nonlinear systems," *Automatica*, 2004.
[24] R. Skjetne, "The maneuvering problem," Ph.D. dissertation, Norwegian University of Science and Technology, 2005.
[25] E. A. Basso, H. M. Schmidt-Didlaukies, K. Y. Pettersen, and A. Sørensen, "Global asymptotic tracking for marine surface vehicles using hybrid feedback in the presence of parametric uncertainties," in *Proc. 2021 American Control Conf.*, New Orleans, LA, USA, 2021.
[26] C. G. Mayhew, R. G. Sanfelice, and A. R. Teel, "Quaternion-based hybrid control for robust global attitude tracking," *IEEE Transactions on Automatic Control*, vol. 56, no. 11, 2011.
[27] F. Bullo and A. D. Lewis, *Geometric Control of Mechanical Systems*. Springer, 2005.
[28] J. M. Selig, *Geometric Fundamentals of Robotics*. Springer, 2004.
[29] T. I. Fossen, *Handbook of Marine Craft Hydrodynamics and Motion Control*, 2nd ed. Wiley, 2020.
[30] G. Antonelli, *Underwater Robots*, 4th ed. Springer, 2018.
[31] R. Goebel, R. G. Sanfelice, and A. R. Teel, *Hybrid Dynamical Systems: Modeling Stability, and Robustness*. Princeton University Press, Princeton, NJ, 2012.
[32] R. G. Sanfelice, *Hybrid Feedback Control*. Princeton University Press, Princeton, NJ, 2021.
[33] B. Paden and R. Panja, "Globally asymptotically stable PD+ controller for robot manipulators," *International Journal of Control*, 1988.
[34] M. Krstic, P. V. Kokotovic, and I. Kanellakopoulos, *Nonlinear and Adaptive Control Design*. John Wiley & Sons, 1995.
[35] R. T. Rockafellar and R. J.-B. Wets, *Variational Analysis*. Springer, 2009.
[36] C. G. Mayhew, R. G. Sanfelice, and A. R. Teel, "On path-lifting mechanisms and unwinding in quaternion-based attitude control," *IEEE Transactions on Automatic Control*, vol. 58, no. 5, pp. 1179–1191, 2013.
[37] Marine Cybernetics Lab, (Accessed Oct. 14th, 2021). [Online]. Available: https://www.ntnu.edu/imt/lab/cybernetics

Erlend A. Basso (GS'19) received the MSc degree in cybernetics and robotics from the Norwegian University of Science and Technology (NTNU), Trondheim, in 2019, where he is currently pursuing a PhD in engineering cybernetics. His current research interests include nonlinear control of mechanical systems, with an emphasis on marine robotics.

Henrik M. Schmidt-Didlaukies (GS'20) received the MSc degree in marine technology from the Norwegian University of Science and Technology (NTNU), Trondheim, in 2017, where he is currently pursuing a PhD in marine technology.

His current research interests include modeling and control of underwater vehicles.

Kristin Y. Pettersen (S'93-M'98-SM'04-F'17) received the MSc and PhD degrees in engineering cybernetics from the Norwegian University of Science and Technology (NTNU), Trondheim, Norway, in 1992 and 1996, respectively. She is a Professor in the Department of Engineering Cybernetics, NTNU, where she has been a faculty member since 1996. She was Head of Department 2011-2013, Vice-Head of Department 2009-2011, and Director of the NTNU ICT Program of Robotics 2010-2013. She is Adjunct Professor at the Norwegian Defence Research Establishment (FFI). In the period 2013 – 2022 she is also Key Scientist at the CoE Centre for Autonomous Marine Operations and Systems. She is a co-founder of the NTNU spin-off company Eelume AS, where she was CEO 2015-2016.

She has published four books and more than 300 papers in international journals and conference proceedings. Her research interests focus on nonlinear control of mechanical systems with applications to robotics, with a special emphasis on marine robotics and snake robotics. She was awarded the IEEE Transactions on Control Systems Technology Outstanding Paper Award in 2006 and in 2017. She was awarded an ERC-AdG-2020 Advanced Grant from the European Research Council, and received the IEEE CSS 2020 Hendrik W. Bode Lecture Prize.

She is a member of the IEEE Control Systems Society Board of Governors 2022 – 2024, and is also a member of the IFAC Council and the EUCA Council. She has also held several board positions in industrial and research companies. She has served as Associate Editor of IEEE Transactions on Control Systems Technology and IEEE Control Systems Magazine, and is currently Senior Editor of IEEE Transactions on Control Systems Technology. She is IEEE CSS Distinguished Lecturer 2019-2021, IEEE Fellow, member of the Norwegian Academy of Technological Sciences, and member of the Academy of the Royal Norwegian Society of Sciences and Letters.

Asgeir J. Sørensen (M'90-SM'19) obtained MSc degree in Marine Technology in 1988 at NTNU, and PhD degree in Engineering Cybernetics at NTNU in 1993. In 1989-1992 Sørensen was employed at MARINTEK (SINTEF) as Research Scientist. In the years 1993-2002 Sørensen was employed in various positions in the ABB Group. In December 2002 Sørensen became co-founder of the company, Marine Cybernetics AS, where he was acting as President and Chief Executive Officer (CEO) until June 2010. In 2012, 2015 and 2017 Sørensen co-founded the companies Ecotone AS, Eelume AS, SES-x Marine Technologies AS and Zeabuz AS, respectively. Since 1999 Sørensen has held the position of Professor of Marine Control Systems at the Department of Marine Technology, NTNU. In the period 2003-2012 he was key scientist in the Centre for Ships and Ocean Structures (CeSOS). He is currently acting as key scientist and the Director of the Centre for Autonomous Marine Operations and Systems (NTNU AMOS) and NTNU VISTA CAROS. Sørensen has authored more than 300 scientific articles and book chapters, and he has graduated more than 100 MSc and 31 PhD candidates. He has also together with colleagues established the Marine Cybernetics Laboratory (MC-Lab) and the Applied Underwater Robotics Laboratory (AUR-Lab), both at NTNU. Sørensen is engaged in bringing fundamental research results into value creation by innovations and entrepreneurships.